The type VII secretion system protects *Staphylococcus aureus* against antimicrobial host fatty acids

Arnaud Kengmo Tchoupa[1], Kate E. Watkins[1], Rebekah A. Jones[1], Agnès Kuroki[2], Mohammad Tauqeer Alam[1], Sebastien Perrier[1,2,3], Yin Chen[4], Meera Unnikrishnan[1*]

[1]Warwick Medical School, University of Warwick, Coventry, United Kingdom

[2]Department of Chemistry, University of Warwick, Coventry, United Kingdom

[3]Faculty of Pharmacy and Pharmaceutical Sciences, Monash University, Parkville, Victoria 3052, Australia

[4]School of Life Sciences, University of Warwick, Coventry, United Kingdom

Running title: *S. aureus* T7SS and fatty acid toxicity

[*]Corresponding author

Email: M.Unnikrishnan@warwick.ac.uk.

Summary

The *Staphylococcus aureus* type VII secretion system (T7SS) exports several proteins that are pivotal for bacterial virulence. The mechanisms underlying T7SS-mediated staphylococcal survival during infection nevertheless remain unclear. Here we show that the absence of EsxC, a small secreted effector implicated in bacterial persistence, results in cell membrane defects in *S. aureus*. Interestingly, isogenic mutants lacking EsxC, other T7SS effectors EsxA and EsxB, or the membrane-bound ATPase EssC, are more sensitive to killing by the host-derived antimicrobial fatty acid, linoleic acid (LA), compared to the wild-type (WT). LA induces more cell membrane damage in the T7SS mutants compared to the WT. Although WT and mutant strains did not differ in their ability to bind labelled LA, membrane lipid profiles show that T7SS mutants are less able to incorporate LA into their membrane phospholipids. Furthermore, proteomic analyses of WT and mutant cell fractions reveal that, in addition to compromising membranes, T7SS defects induce oxidative stress and hamper their response to LA challenge. Thus, our findings indicate that T7SS is crucial for *S. aureus* membrane integrity and homeostasis, which is critical when bacteria encounter antimicrobial fatty acids.

Keywords: *Staphylococcus aureus*, Type VII secretion system, long-chain unsaturated free fatty acids.

41 **Introduction**

42 *Staphylococcus aureus* is a facultative pathogen that can colonize the skin and nares
43 of healthy individuals. The asymptomatic carriage of *S. aureus* is a major risk for
44 subsequent infections (von Eiff *et al.*, 2001). *S. aureus* infections, which can be
45 healthcare or community-associated, range from benign impetigo to life-threatening
46 bacteraemia (Tong *et al.*, 2015). Clinical management of staphylococcal infections is
47 complicated by the increasing prevalence of multidrug resistant strains (Lee *et al.*,
48 2018).

49 The success of *S. aureus* as a deadly pathogen is attributed to an array of virulence
50 factors that facilitate host tissue adhesion and immune response evasion (Gordon &
51 Lowy, 2008). One of these virulence factors is the type VII secretion system (T7SS),
52 also known as the ESAT-6 secretion system (ESS). The orthologous ESX-1 system
53 was initially discovered in *Mycobacterium tuberculosis*, where it is essential for
54 bacterial virulence (Conrad *et al.*, 2017). T7SSs (T7SSb) are found in both Gram-
55 positive and Gram-negative bacteria, although these systems and their secretion
56 machineries appear to be distinct to their mycobacterial counterparts (Unnikrishnan *et*
57 *al.*, 2017).

58 In extensively studied strains (COL, RN6390, USA300 and Newman), the T7SS
59 consists of four integral membrane proteins (EsaA, EssA, EssB and EssC), two
60 cytosolic proteins (EsaB and EsaG), five secreted substrates (EsxA, EsxB, EsxC,
61 EsxD and EsaD), and EsaE, which interacts with the T7SS substrates to target them
62 to the secretion apparatus (Cao *et al.*, 2016). A peptidoglycan hydrolase, EssH, was
63 reported to mediate T7SS transport across the bacterial cell wall envelope
64 (Bobrovskyy *et al.*, 2018).

65 The molecular architecture of the staphylococcal T7SS has not yet been fully
66 characterized. T7SS integral membrane proteins EsaA, EssA, EssB, and EssC are
67 thought to be the core of the T7 secretion machinery, with EssC being the central
68 membrane transporter (Burts *et al.*, 2005, Jager *et al.*, 2018, Zoltner *et al.*, 2016).
69 Interactions between secreted substrates and co-dependent secretion of substrates
70 have been demonstrated (Anderson *et al.*, 2013, Cao *et al.*, 2016, Kneuper *et al.*,
71 2014, Ohr *et al.*, 2017). A recent study showed that the functional assembly of the
72 T7SS machinery in *S. aureus* is supported by the flotillin homolog FloA, within
73 functional membrane microdomains (Mielich-Suss *et al.*, 2017).

74 The *S. aureus* T7SS is pivotal for bacterial virulence. Indeed, S. *aureus* mutants
75 lacking the entire T7SS (Kneuper *et al.*, 2014) or specific T7SS components (EsxA,
76 EssB, EssC, EsxC, EsxB, EsaB, EsaD or EsaE) were consistently shown to be less
77 virulent and/or persistent in various mouse infection models (Anderson *et al.*, 2011,
78 Anderson *et al.*, 2017, Burts *et al.*, 2008, Burts *et al.*, 2005, Ishii *et al.*, 2014, Lopez *et*
79 *al.*, 2017). EsxA is necessary to delay apoptosis of *S. aureus*-infected epithelial and
80 dendritic cells, while other substrates modulate cytokine production (Anderson *et al.*,
81 2017, Cruciani *et al.*, 2017, Korea *et al.*, 2014). Although the relevance of T7SS to *S.*
82 *aureus* is less understood, a role for the toxin-antitoxin pair EsaD (or EssD) and EsaG
83 (or EssI) was recently demonstrated in intraspecies competition (Cao *et al.*, 2016, Ohr
84 *et al.*, 2017).

85 Interestingly, *S. aureus* T7SS expression is induced in response to host-specific FAs
86 (Ishii *et al.*, 2014, Kenny *et al.*, 2009, Lopez *et al.*, 2017), although the role of T7SS in
87 bacterial resistance to antimicrobial FAs remains unclear. In this study, we
88 demonstrate that *S. aureus* lacking the T7SS substrate EsxC has a defective cell
89 membrane. Intriguingly, EsxC and other T7SS mutants were more sensitive to an

90 unsaturated FA, linoleic acid (LA), compared to the wild-type (WT). Although there
91 were no differences in binding labelled LA, LA induced a more leaky membrane in the
92 T7SS mutants, and there was less incorporation of LA into membrane phospholipids.
93 Cellular proteomics revealed that in addition to membrane discrepancies, T7SS
94 mutants exhibited different redox and metabolic states, which likely result in a distinct
95 response to LA.

96

97 **Results**

98 **The type VII substrate EsxC is present on the staphylococcal surface and affects**
99 **its composition**

100 EsxC, a small 15-kDa protein secreted by the T7SS, is important for *S. aureus*
101 persistence in mice (Burts *et al.*, 2008). However, mechanisms underlying EsxC- or
102 T7SS-mediated bacterial survival are not known. In order to understand the role of
103 EsxC, we generated an isogenic *esxC* mutant as described previously (Bae &
104 Schneewind, 2006), and confirmed the absence of any secondary site mutations by
105 whole genome sequencing. Δ*esxC* had a similar growth rate to the WT USA300 JE2
106 strain (Fig. S1). EsxC is known to be a secreted effector of T7SS (Burts *et al.*, 2008),
107 although it has been consistently detected in cell membrane (CM) fractions of RN6390
108 and USA300 (Bobrovskyy *et al.*, 2018, Kneuper *et al.*, 2014). As reported previously,
109 we detected EsxC in the CM fractions of the WT but not in Δ*esxC* (Fig. S2). Moreover,
110 we also detected EsxC in the WT cell wall (CW) fraction (Fig. S2). In a deletion mutant
111 of the membrane-bound major ATPase EssC (a core T7SS component), EsxC was
112 detected in CM and CW preparations even in the absence of EssC (Fig. S2). While
113 we were unable to detect EsxC in the cell-free supernatants by immunoblotting, we

114 detected this protein by secretome analyses. Along with EsxC, other T7SS proteins,
115 EsxA and EsxD, were detected in the WT but not in Δ*esxC or* Δ*essC* supernatants
116 (Table S1).

117 Given the association of EsxC with the cell membrane, we stained the WT, Δ*esxC* and
118 Δ*essC* mutants with FM-143, a fluorescent cell membrane probe (Pulschen *et al.*,
119 2017). We observed a mild but statistically significant increase in FM-143 staining in
120 the mutants as compared to the WT (Fig. 1A). Increased staining of membranes by
121 FM-143 has been associated previously with membrane blebbing in bacteria (Wood
122 *et al.*, 2019).

123 To study if the lack of T7SS proteins affected other surface proteins, a surface
124 proteome analysis of the WT and mutants was carried out using trypsin treatment to
125 digest surface proteins (Solis *et al.*, 2014). We found that most proteins (172/218) were
126 less abundant in Δ*esxC* compared to the WT (Fig. S3). Interestingly, majority of
127 relatively less abundant proteins (16/20) in the Δ*esxC* surface proteome were
128 predicted or proven to be cytosolic (Table S2). Metabolic (PfKA, FolD, FabI GatB, and
129 ImdH) or stress-related (Asp23 and putative universal stress proteins) proteins were
130 lowest in abundance ($\log_2$ fold change < - 1.0). The T7SS core component EsaA, which
131 has a prominent extracellular loop (Dreisbach *et al.*, 2010), was also ~50% less
132 abundant in Δ*esxC*, implying that EsxC absence may affect T7SS assembly.
133 Identification of cytosolic proteins during surface proteome analysis could be attributed
134 to non-canonical secretion of cytosolic proteins that bind to bacterial surfaces (Hempel
135 *et al.*, 2011, Pasztor *et al.*, 2010) or cell lysis during sample preparation (Dreisbach *et*
136 *al.*, 2010, Solis *et al.*, 2014, Ventura *et al.*, 2010). To study if the T7SS mutants were
137 more resistant to cell lysis, we compared the Triton X-100 lysis of WT, Δ*esxC* and,

138 Δ*essC* in PBS in non-growing conditions. While Δ*esxC* was slightly more resistant to
139 Triton X-100, Δ*essC* was clearly defective in lysis (Fig. 1B), as compared to the WT.

140 We probed T7SS effects on the membrane further by assessing membrane fluidity of
141 the WT and Δ*esxC* mutant. We used pyrene decanoic acid, an eximer-forming lipid
142 (Lopez *et al.*, 2017), to measure the fluidity of WT and Δ*esxC* membranes. Compared
143 to the WT, the cytosolic membrane of the Δ*esxC* mutant showed a mild but statistically
144 significant increase in rigidity (Fig. 1C). Furthermore, we stained WT and with a
145 fluorescent membrane dye DiI12C, which has been used detect regions of increased
146 fluidity in bacteria (Saeloh *et al.*, 2018). As reported previously for *S. aureus*, we
147 observe few fluid regions in the WT, and an uneven staining of the membrane. In
148 contrast, a very weak staining of the membranes was observed for the Δ*esxC* mutant,
149 (Fig 1 D and E), which may indicate a decrease in membrane fluidity.

150 Overall, the data indicate that EsxC contributes to *S. aureus* cell surface structure and
151 membrane fluidity.

152

153 ***S. aureus esxC* and *essC* mutants are more sensitive to antimicrobial fatty acids**

154 Multiple studies have reported the activation of the T7SS, when *S. aureus* is grown in
155 presence of host FAs (Ishii *et al.*, 2014, Kenny *et al.*, 2009, Lopez *et al.*, 2017). Given
156 our findings that the *esxC* mutant has membrane defects and that the *esxC* deletion
157 affects the surface abundance of IsdA, which is essential for *S. aureus* resistance to
158 antimicrobial fatty acids (Clarke *et al.*, 2007), we cultured WT USA300 and its isogenic
159 *essC* or *esxC* mutant in the presence of an unsaturated FA (C18:2), linoleic acid (LA),
160 at a concentration (80 μM) that still allows WT growth. Bacteria were also cultured in
161 parallel in presence of stearic acid (SA), a saturated C18:0 FA. The T7SS mutants

162 displayed impaired growth in presence of LA but not SA, as measured by optical
163 density (OD) (Fig. 2A) or colony forming units (CFU) (Fig. 2B). Importantly, Δ*esxC*
164 complemented with a plasmid containing the *esxC* gene reverted to the WT phenotype
165 (Fig. 2C). The increased susceptibility of T7SS mutants to antimicrobial fatty acids was
166 not restricted to linoleic acid; when cultured in the presence of arachidonic acid,
167 another unsaturated FA (C20:4), growth of Δ*esxC* and Δ*essC* were inhibited more as
168 compared to the WT (Fig. S4)

169

170 **T7SS substrates contribute to *S. aureus* resistance to LA toxicity**

171 Next, we investigated whether T7SS proteins other than *essC* and *esxC* contributed
172 to *S. aureus* growth in presence of LA. Mutants lacking two other substrates, Δ*esxA*
173 and Δ*esxB*, were grown in presence of FAs. Both mutants grew slower than the WT
174 USA300 (Fig. S5A). To ensure that the increased sensitivity observed for the T7SS
175 mutants was not strain specific, RN6390 Δ*essC* or Δ*esxC* and Newman Δ*esxA* or
176 Δ*esxB* mutants were tested. Similar to the USA300 mutants, the growth of all these
177 T7SS mutants was also impacted in the presence of LA (Fig. S5B and C). The growth
178 defect in Newman Δ*esxA* was abrogated upon complementation (Fig. 2D). Of note,
179 the Newman WT was readily inhibited by a lower concentration of LA (40 μM), which
180 is in agreement with the lower T7SS expression levels in this strain compared to
181 USA300 (Anderson *et al.*, 2013, Kneuper *et al.*, 2014). We conclude that a functional
182 T7SS plays a role in *S. aureus* resistance to LA toxicity.

183

184 **T7SS is required for maintaining membrane integrity in presence of LA**

185 To study the mechanisms involved in T7SS mediated protection to LA toxicity, further
186 studies were performed using strains lacking esxC, a representative T7SS effector, or
187 essC the main T7SS transporter. As our membrane and surface proteome analyses
188 with Δ*esxC* suggested that the bacterial envelope is altered upon T7SS defect, we
189 wanted to test if LA-mediated growth inhibition was due to an increased binding of LA
190 to T7SS mutants. To do this, we chemically engineered LA to produce an azide
191 functionalised LA (N^6-diazo-N^2-((9Z,12Z)-octadeca-9,12-dienoyl)lysine, N_3-LA) or
192 azide-LA (Fig. 3A). After incubating bacteria with azide-LA, click-chemistry with an
193 alkyne dye (Click-iT™ Alexa Fluor™ 488 sDIBO alkyne) was used to stain azide-LA
194 associated with bacteria. There were no obvious differences in the fluorescence from
195 Δ*essC* and Δ*esxC* compared to the WT (Fig. 3B), suggesting that T7SS components
196 are not involved in binding or sequestering LA. However, when bacteria treated with
197 azide-LA were stained with propidium iodide (PI), a good indicator of membrane
198 integrity, Δ*essC* and Δ*esxC* displayed a more intense PI staining compared to the WT
199 (Fig. 3C and D). Similarly, when WT and mutants were stained with PI and SYTO 9
200 after treatment with 80 µM unlabelled LA, we observed an increased PI staining (Fig.
201 4A and B) and therefore lower SYTO 9 / PI (Live/Dead) ratio for both mutants (Figure
202 4C). These data suggest that an intact T7SS helps *S. aureus* to maintain its membrane
203 integrity when faced with the detergent-like effects of unsaturated FAs.

204

205 **LA-incorporation into membrane phospholipids is modulated by T7SS**

206 As the T7SS mutants have more compromised cell membranes in presence of LA, we
207 next investigated if membrane lipids were altered in the T7SS mutants. Lipids from
208 WT USA300 and T7SS mutants were analysed by high-performance liquid

209 chromatography (HPLC)-mass spectrometry (MS) in negative ionisation mode. As
210 reported previously (Delekta *et al.*, 2018, Parsons *et al.*, 2011), phosphatidylglycerol
211 (PG) was the major phospholipid present in the membrane of WT grown in TSB (Fig.
212 S6A). Δ*essC* and Δ*esxC* grown with or without 10 μM LA [(a concentration that has
213 been previously shown to be sub-inhibitory for USA300 (Lopez *et al.*, 2017)] displayed
214 lipid profiles similar to that of WT (Fig. S6A and B). Notably, PG molecular species
215 were significantly altered upon growth in LA-supplemented TSB for WT (Fig. 5A),
216 Δ*essC* (Fig. S6C) and Δ*esxC* (Fig. 5B). Three new LA-specific PG species with mass
217 to charge ratios (m/z) 731 (C33:2), 759 (C35:2), and 787 (C37:2) appeared to contain
218 LA (C18:2) or its elongated C20:2 or C22:2 versions, as revealed by their
219 fragmentations (Fig. S7A, B and C). PG species containing exogenous, unsaturated
220 FAs were also present in Δ*essC* and Δ*esxC*. However, LA (C18:2)-containing PG
221 species (C33:2) were less abundant in the *esxC* mutant compared to WT (Fig. 5C). A
222 similar trend, although statistically non-significant ($P > 0.05$), was observed for C20:2-
223 and C22:2-containing PG species (Fig. S7D and E), and when all the unsaturated
224 exogenous PG species were combined (Fig. 5D). The data suggest that a T7SS defect
225 may compromise the incorporation and elongation of LA in *S. aureus* membranes.

226

227 **T7SS mutations affect the total cellular content and *S. aureus* responses to LA**

228 In order to gain further insight into T7SS-mediated modulation of proteins involved in
229 FA incorporation and membrane homeostasis in presence of LA, we used an unbiased
230 proteomic approach to study protein profiles of WT USA300, Δ*essC*, and Δ*esxC* grown
231 exponentially with or without 10 μM LA. Of note, WT and both these T7SS mutants
232 grew similarly in presence of up to 40 μM LA (Fig. S8).

233 *WT vs T7SS mutants in absence of LA treatment:* Interestingly, Δ*essC* or Δ*esxC*
234 cultured in TSB readily displayed proteins with changed abundance when compared
235 to the WT, with 37 and 24 proteins significantly ($P < 0.05$) altered in Δ*essC* and Δ*esxC*,
236 respectively. Similarly, 14 proteins were differentially abundant in both Δ*essC* and
237 Δ*esxC* (Fig. 6A and B). These included proteins associated with signal transduction
238 (LytR and ArlR), the CW (acetyltransferase GNAT, FnbB and MazF), DNA repair (MutL
239 and RadA), nucleotide binding (ATP-grasp domain protein and YqeH), hydrolysis
240 (amidohydrolase), cell stress response [universal stress protein (Usp) family], or were
241 uncharacterised (A0A0H2XGJ8, YbbR and lipoprotein) (Fig. 6B and Table 1). Of the
242 33 proteins changed only in Δ*essC* (23 proteins) or Δ*esxC* (10 proteins), nearly 40%
243 (13 proteins) were associated with oxidation-reduction and other metabolic processes.
244 Ten membrane proteins were more abundant in Δ*essC* (Table 1), which included SrrB,
245 a membrane protein that is activated by impaired respiration (Mashruwala *et al.*, 2017),
246 and whose gene expression increased 6 times upon growth in presence of LA (Lopez
247 *et al.*, 2017). SrrB was also detected at higher levels in the *esxC* mutant although the
248 increase was non-significant ($P = 0.07$).

249 **Table 1. Proteins with changed abundance in Δ*essC* and Δ*esxC* mutants relative to the WT**
250 **USA300 JE2**

		Δ*essC*/WT		Δ*esxC*/WT		
Functions	**Uniprot ID**	**Log_2 FC**	**Adjusted *P* value**	**Log_2 FC**	**Adjusted *P* value**	**Description**
Signal transduction systems	Q2FK09	-3.0	4.90E-13	-3.1	4.90E-13	Sensory transduction protein LytR
	Q2FH23	-2.9	0.002527	-2.1	0.026184	Response regulator ArlR
Membrane proteins	A0A0H2XF42	3.0	1.75E-10	0	1	Cytochrome D ubiquinol oxidase, subunit I
	A0A0H2XDZ5	1.7	1.68E-05	0	1	Uncharacterized membrane protein
	A0A0H2XFJ8	2.0	0.001077	0.5	0.883953	Uracil permease
	A0A0H2XGW7	2.7	0.005757	2.5	0.010784	Putative lipoprotein
	A0A0H2XIA9	1.0	0.006115	0	1	Protein translocase subunit SecY
	Q2FIN2	1.6	0.029451	0.5	0.970614	Prolipoprotein diacylglyceryl transferase LGT
	A0A0H2XKD9	2.0	0.038093	1.8	0.070347	Staphylococcal respiratory response protein SrrB
	A0A0H2XFE1	3.4	0.039814	1.1	0.970614	Peptidase
	A0A0H2XJV8	2.0	0.04444	1.5	0.231285	Cyclic-di-AMP phosphodiesterase
	A0A0H2XGF4	3.0	0.044681	0.9	0.986458	Sodium:dicarboxylate symporter family protein
	A0A0H2XHV2	2.5	0.049168	2.4	0.070182	Glycine betaine transporter OpuD
Stress response	A0A0H2XKH6	2.2	5.80E-05	2.5	1.07E-05	Universal stress protein family
	A0A0H2XIZ0	0.0	1	-3.4	1. 06E-10	OsmC/Ohr family protein
DNA repair	Q2FHE2	-2.3	1.79E-08	-2.3	1.19E-08	DNA mismatch repair protein MutL
	A0A0H2XI63	-2.0	0.004036	-2.0	0.004036	DNA repair protein RadA
	A0A0H2XHT1	-0.3	0.708343	-1.9	0.008379	Formamidopyrimidine-DNA glycosylase MutM
Oxidation-reduction process	A0A0H2XJ90	1.1	0.038093	1.0	0.088334	D-isomer specific 2-hydroxyacid dehydrogenase family protein
	A0A0H2XHE0	2.4	0.039099	-0.1	1	Thiol-disulphide oxidoreductase, DCC family protein
	A0A0H2XGR9	0.0	1	1.4	8.89E-08	Oxidoreductase, Gfo/Idh/MocA family
	A0A0H2XK08	1.0	0.406975	2.9	0.00791	Oxidoreductase, short chain dehydrogenase/reductase family
	A0A0H2XFZ3	-0.8	0.404225	2.1	0.016405	Nitroreductase family protein
Hydrolases	A0A0H2XE49	2.9	1.07E-06	2.9	5.99E-07	Amidohydrolase
	Q2FES9	-2.7	0.003385	-0.3	1	Uncharacterized hydrolase
	A0A0H2XFF2	-0.8	0.016697	-0.5	0.157809	Peptidase, U32 family
	A0A0H2XJH8	0.0	1	2.8	1.06E-10	Peptidase M20 domain-containing protein 2
	A0A0H2XJ54	0.0	1	2.0	0.000949	Hydrolase (HAD superfamily)
	Q2FEG2	-0.2	0.854748	-2.9	0.004615	Formimidoylglutamase
Metabolism	A0A0H2XGU2	-1.6	4.99E-06	-0.1	1	Pseudouridine synthase
	A0A0H2XK15	2.8	0.004424	0.9	0.777138	1-phosphatidylinositol phosphodiesterase
	Q2FEK2	-1.6	0.038093	-0.3	1	Urease accessory protein UreE
	Q2FI05	1.1	0.038093	0.0	1	Bifunctional purine biosynthesis protein PurH
	Q2FIL2	2.9	0.038093	0.8	0.970614	SsrA-binding protein
	A0A0H2XII6	1.8	0.038093	1.5	0.088334	Orn/Lys/Arg decarboxylase
	A0A0H2XJR8	-0.9	0.04444	-0.5	0.61246	RNA methyltransferase, RsmD family
	A0A0H2XKG7	0.0	1	1.4	8.18E-08	Aspartokinase
Cell wall composition	A0A0H2XJQ4	-4.0	4.92E-11	-4.0	3.28E-11	Acetyltransferase, GNAT family
	A0A0H2XKG3	-2.3	0.001238	-1.7	0.016405	Fibronectin binding protein B
	A0A0H2XJC8	-2.3	0.009779	-3.0	0.000819	Phi77 ORF017-like protein (Toxin MazF)
	Q2FE03	0.0	1	2.6	1.18E-12	Fibronectin-binding protein A
Nucleotide binding	A0A0H2XHY5	-2.3	8.58E-06	-2.3	6.01E-06	ATP-grasp domain protein
	A0A0H2XFA5	3.3	0.014259	3.5	0.008379	Putative GTP-binding YqeH protein
Uncharacterised proteins	A0A0H2XGJ8	2.2	0.000372	2.4	9.41E-05	Uncharacterized protein
	A0A0H2XE09	2.1	0.008231	1.9	0.016405	Ybbr-like uncharacterized protein
	Q2FFI4	3.4	0.020136	0.9	0.970614	UPF0316 membrane protein
	A0A0H2XG24	1.1	0.022345	0.8	0.088334	Uncharacterized protein

251 *WT vs T7SS mutants in presence of LA*: We then compared the proteomic profiles of
252 LA-treated strains (WT, Δ*essC* or Δ*esxC*) with their untreated counterparts. Clearly,
253 the principal component analysis revealed that the differences due to the genetic
254 makeup (WT or T7SS mutants) were less prominent than the dramatic changes
255 induced by LA (Fig. S9). These changes are exemplified for the WT; 163/1132 proteins
256 identified had an altered relative abundance upon growth with LA (Fig. 6C). 167 and
257 171 proteins were changed ($P < 0.05$) in Δ*essC* and Δ*esxC*, respectively, in response
258 to LA, of which ~ 40% (68 proteins) were common to these mutants and their WT (Fig.
259 6D). At least 30% of the significantly changed proteins ($P < 0.05$) were unique to WT
260 (53 proteins), Δ*essC* (50 proteins), or Δ*esxC* (64 proteins) (Fig. 6D), suggesting that
261 each strain responds differently to LA. However, almost all proteins (13/14 proteins)
262 that were similarly deregulated in Δ*essC* and Δ*esxC* grown without LA (Fig. 6B) were
263 modulated in presence of LA (highlighted in bold in Dataset S1). Proteins that were
264 less abundant in both mutants were, upon LA treatment, either increased to WT levels
265 (MutL, acetyltransferase GNAT, Toxin MazF, and ATP-grasp domain protein), or were
266 unchanged in the mutants and decreased in the LA-treated WT (LytR and FnbB)
267 (Dataset S1). Likewise, proteins with increased amounts in Δ*essC* or Δ*esxC* were: (i)
268 downregulated to WT levels in response to LA (putative lipoprotein A0A0H2XGW7),
269 (ii) unaltered in both mutants and upregulated in WT (Usp, amidohydrolase, and
270 YbbR), (iii) or further increased in the *essC* mutant and strongly upregulated in WT
271 (A0A0H2XGJ8) (Dataset S1). In sum, except for ArlR and RadA that were conversely
272 regulated in all strains after LA treatment, proteins similarly deregulated in Δ*esxC* and
273 Δ*essC* were returned to similar levels in response to LA. A similar trend was observed
274 for 15/23 and all 10 proteins exclusively more or less abundant in Δ*essC* and Δ*esxC*,
275 respectively.

276 *Altered molecular functions in presence of LA:* We then used QuickGO (a web-based
277 tool for Gene Ontology searching) (Binns *et al.*, 2009) to retrieve GO terms associated
278 with the ten most significantly upregulated proteins in LA-treated WT (Dataset S1).
279 Strikingly, 9/10 proteins had a hydrolase or an oxidoreductase activity. A
280 comprehensive, statistical analysis showed a clear enrichment of 8 specific molecular
281 functions ($P < 0.05$) in at least one strain (WT or T7SS mutants) (Fig. 7A).
282 Oxidoreductase and hydrolase activities were enhanced in LA-treated WT, while
283 Δ*essC* and Δ*esxC* were less able to upregulate proteins with these molecular
284 functions. Flavin adenine dinucleotide (FAD)-binding, which plays a role in oxidation-
285 reduction and FA metabolic processes, was similarly more enriched in the LA-treated
286 WT. In contrast, transferase activity, which is linked to CW synthesis, was induced
287 more in T7SS mutants compared to the WT. Molecular functions that are decreased
288 upon LA challenge were also determined (Fig. 7B). In agreement with reduced
289 intracellular ATP levels following membrane damage by antimicrobial FAs (Cartron *et*
290 *al.*, 2014), genes with the ATP-binding function (mainly ATP-binding ABC transporters)
291 were strongly inhibited in the WT. ATP-dependent lyases were also repressed in the
292 WT. On the contrary, T7SS mutants were less able to modulate ATP-binding proteins.
293 Instead, a strong inhibition of ribosomal constituents and other translation-related
294 components was seen (Fig. 7B).

295 To test the oxidoreductive states of the WT and the mutants, we stained bacteria with
296 dichlorofluorescin (DCF), which detects reactive oxygen species (George *et al.*, 2019).
297 Reflecting the changes seen in the proteomics data, when treated with 10 μM LA there
298 is an increase in the ROS generated in the T7SS mutants compared to the WT (Fig
299 7C). However, in bacteria grown without LA, the mutants have slightly less or no
300 change in the ROS generated compared to WT (Figure 7D). Taken together, our

301 proteomic analyses reveal that the lack of T7SS induces altered membrane and
302 metabolic states indicative of oxidative stress responses. While the WT shows a
303 multifaceted response to mitigate LA-induced damage on the bacterial membrane,
304 such responses are clearly altered in the absence of the T7SS.

305

306 **Discussion**

307 Host fatty acids (FAs) play a crucial role in the host defence to *S. aureus* infections. *S.*
308 *aureus* is particularly sensitive to unsaturated FAs, which are abundant in the human
309 skin (Clarke *et al.*, 2007, Parsons *et al.*, 2012, Arsic *et al.*, 2012, Kelsey *et al.*, 2006,
310 Kenny *et al.*, 2009). We report here that the T7SS, an important component of *S.*
311 *aureus* virulence arsenal, is critical in modulating the response to antimicrobial host
312 FAs by maintaining the bacterial cell membrane integrity. Specifically, we demonstrate
313 that a T7SS substrate, EsxC, impacts *S. aureus* membrane properties. A functional
314 T7SS enables bacteria to mitigate LA-induced toxicity and grow better than mutants
315 with a compromised T7SS. In the absence of T7SS components, LA is less
316 incorporated into membrane phospholipids and enhances cell membrane damage,
317 while bacteria are unable to activate adaptive mechanisms involved in LA resistance,
318 as indicated by cellular proteomics.

319 Although several studies have shown multiple interactions between the staphylococcal
320 T7SS components, the precise molecular architecture of this system remains unclear.
321 EsxC (previously EsaC) was first described as a secreted protein (Burts *et al.*, 2008).
322 However, in keeping with prior studies, we found that EsxC can also localize within
323 staphylococcal membranes (Bobrovskyy *et al.*, 2018, Kneuper *et al.*, 2014). Based on
324 available data, EsxC is likely to be associated to EsxA, EsaD, or EsaE on the

325 membrane (Anderson *et al.*, 2013, Anderson *et al.*, 2017, Cao *et al.*, 2016).
326 Additionally, the reduced EsaA protein levels that we found on the surface of *S. aureus*
327 USA300 Δ*esxC* combined with prior observations of diminished EsxC protein levels in
328 RN6390 Δ*esaA* membranes (Kneuper *et al.*, 2014) suggest that EsxC may interact
329 with EsaA, a key component of the T7SS core (Aly *et al.*, 2017), in *S. aureus*
330 membranes.

331 T7SS integral membrane proteins interact with the flotillin homolog FloA within
332 functional membrane microdomains (FMMs) (Mielich-Suss *et al.*, 2017). FMMs were
333 recently shown to contain staphyloxanthin derivatives (Garcia-Fernandez *et al.*, 2017),
334 which are known to increase membrane rigidity (Chamberlain *et al.*, 1991, Sen *et al.*,
335 2016, Tiwari *et al.*, 2018). Hence, well-structured FMMs may play a role in *S. aureus*
336 membrane fluidity as reported for *Bacillus subtilis* (Bach & Bramkamp, 2013).
337 Interestingly, mutations or treatments affecting *S. aureus* membrane fluidity also
338 modulate T7SS transcription (Lopez *et al.*, 2017, Ishii *et al.*, 2014, Parsons *et al.*,
339 2014). Hence, there appears to be a link between membrane fluidity and T7SS in *S.*
340 *aureus*. Also, the state of the membrane was suggested to trigger the production of
341 T7SS (Lopez *et al.*, 2017). Remarkably, deletion of *esxC* led to a mild increase in
342 bacterial membrane rigidity and membrane defects (Fig. 1), suggesting membrane
343 modulation by the T7SS. Possibly, interactions between FloA and T7SS are perturbed
344 upon *esxC* deletion and affect *S. aureus* FMMs. We surmise that a functional T7SS
345 helps *S. aureus* to maintain its membrane architecture.

346 The current cellular proteomics data reveal that the abundance of more proteins is
347 altered in Δ*essC* (37) than *esxC* (24) in comparison to *S. aureus* WT, which is in
348 keeping with the greater importance of EssC as the conserved driving force of the
349 T7SS (Warne *et al.*, 2016). Importantly, almost 60% of proteins deregulated in Δ*esxC*

350 are similarly affected in Δ*essC*, strongly suggesting that any modification of the T7SS
351 core leads to a similar staphylococcal response. Surprisingly, proteins with altered
352 abundance in USA300 Δ*essC* were distinct to the ferric uptake regulator (Fur)-
353 controlled genes differentially expressed in RN6390 Δ*essC* (Casabona *et al.*, 2017b).
354 This discrepancy might be due to strain differences, including *rsbU* defect in RN6390
355 that impairs SigB activity (Cassat *et al.*, 2006, Giachino *et al.*, 2001). Nevertheless,
356 given the known role of Fur in oxidative stress resistance (Horsburgh *et al.*, 2001,
357 Johnson *et al.*, 2011), both mutants may display an altered oxidative status following
358 *essC* deletion. *S aureus* RN6390 also differentially expresses redox-sensitive genes
359 in absence of EsaB (Casabona *et al.*, 2017a). Also, since the T7SS substrate EsxA is
360 upregulated in response to hydrogen pyroxide (Casabona *et al.*, 2017b), one could
361 speculate that lack of T7SS stimulates an oxidative stress response. A further
362 indication of altered physiological states of Δ*essC* and Δ*esxC* was the decreased
363 abundance of the two-component regulatory system proteins, LytSR, ArlSR and
364 SrrAB, which was consistent with down-regulation of *lytR* transcription observed
365 previously in the absence of *arlR* (Liang *et al.*, 2005). Importantly, the *S. aureus*
366 response to antimicrobial FAs includes downregulation of *lytRS* (Kenny *et al.*, 2009,
367 Neumann *et al.*, 2015), and upregulation of *srrB* (Lopez *et al.*, 2017). Given that LytSR
368 is involved in bacterial surface and membrane potential modulation (Patton *et al.*,
369 2006, Groicher *et al.*, 2000), T7SS defects are likely to result in an altered cell
370 envelope.

371 It is striking that the staphylococcal T7SS is strongly upregulated in presence of sub-
372 inhibitory concentrations of LA (Kenny *et al.*, 2009, Lopez *et al.*, 2017). FAs with more
373 cis double bonds, which are more toxic toward *S. aureus* (Parsons *et al.*, 2012), are
374 also more potent T7SS activators (Lopez *et al.*, 2017). Our current study interestingly

375 suggests a protective role of T7SS against LA toxicity. Previously described *S. aureus*
376 antimicrobial FA (AFA) resistance mechanisms, including IsdA or wall teichoic acid-
377 mediated modulation of cellular hydrophobicity (Clarke *et al.*, 2007, Kohler *et al.*, 2009,
378 Parsons *et al.*, 2012, Moran *et al.*, 2017), and AFA detoxification with the efflux pumps
379 Tet38 and FarE (Alnaseri *et al.*, 2015, Truong-Bolduc *et al.*, 2014), do not appear to
380 explain the increased susceptibility of T7SS mutants to LA, as indicated by cellular
381 proteomics. In line with a role for T7SS in the oxidative stress response, T7SS mutants
382 were less able to prime their redox-active proteins in response to LA-induced oxidative
383 stress. Instead, to cope with LA, they appear to rely on strong inhibition of the protein
384 synthesis machinery, which is reminiscent of the stringent response (Geiger *et al.*,
385 2012).

386 The Fak pathway which is required for incorporation of exogenous FA into membrane
387 phospholipids via a two-component fatty acid kinase (Fak) (Nguyen *et al.*, 2016,
388 Parsons *et al.*, 2012, Parsons *et al.*, 2014), was reported to be important for T7SS
389 activation by unsaturated FA (Lopez *et al.*, 2017). FakB1 and FakB2, bind to FAs, and
390 FakB-bound FAs are phosphorylated by FakA prior to their incorporation (Parsons *et*
391 *al.*, 2014). In presence of inhibitory concentrations of unsaturated FA like LA, while FA
392 is incorporated into the membrane lipids, free LA causes pore formation that leads to
393 bacterial lysis (Greenway & Dyke, 1979). Our lipidomic analyses revealed that in the
394 absence of T7SS, bacteria were less able to incorporate LA into their phospholipids
395 (Figure 5), and displayed an increased membrane permeability in presence of LA.
396 However, it seems counterintuitive that LA incorporation was impacted more in Δ*esxC*
397 than in Δ*essC* given the central role of EssC in T7 secretion (Burts *et al.*, 2005, Jager
398 *et al.*, 2018, Zoltner *et al.*, 2016). It is possible that EsxC that accumulates in the
399 membrane (Fig. 1A) in the absence of protein secretion by the main transporter, EssC,

400 mediates partial LA incorporation in the *essC* mutant; secretion per se may not be
401 required for LA incorporation. It is also worth noting that transcript levels of *esxC*, and
402 not *essC*, were strongly upregulated in a *S. aureus fakA* mutant (Parsons *et al.*, 2014).
403 As protein levels of Fak proteins in the T7SS mutants stay unaltered in presence or
404 absence of LA, suggesting no T7SS-mediated regulatory control of the Fak pathway,
405 we speculate that EsxC and other interdependent T7SS substrates play an important
406 role in facilitating Fak function in *S. aureus* membranes, either by mediating
407 recruitment or targeting of Fak proteins to the membrane. Our findings warrant further
408 investigations into molecular mechanisms underlying T7SS-mediated FA
409 incorporation within staphylococcal membranes.

410 The increased susceptibility of T7SS mutants to LA might explain why they are less
411 virulent in environments rich in LA and other AFAs like the mouse lungs (Δ*essC*) (Ishii
412 *et al.*, 2014), abscesses (Δ*esxC* and Δ*esaB*), liver and skin (Δ*essB*) (Wang *et al.*, 2016,
413 Lopez *et al.*, 2017). Previous research showing T7SS induction by host-derived FAs
414 further supports the importance of T7SS in such environments (Lopez *et al.*, 2017,
415 Ishii *et al.*, 2014). Taken together, we conclude that T7SS plays a key role in
416 modulating the *S. aureus* cell membrane in response to toxic host FAs. Although, at
417 present, it is unclear how T7SS contributes to staphylococcal membrane architecture,
418 T7SS interaction with the flotillin homolog FloA within functional membrane
419 microdomains (Mielich-Suss *et al.*, 2017) corroborates the idea that T7SS proteins
420 interact with many other proteins to modulate *S. aureus* membranes. Indeed, our data
421 also suggest that blocking T7SS activity would make *S. aureus* more vulnerable to
422 AFAs, a key anti-staphylococcal host defence, thus making T7SS a very attractive
423 drug target.

424 **Experimental procedures:**

425 **Bacterial strains and growth conditions.** *S. aureus* strains used are listed in Table
426 S3, and were grown aerobically in tryptic soy broth (TSB) overnight (O/N) at 37ºC for
427 each experiment unless stated otherwise. For complemented *S. aureus* strains, TSB
428 was supplemented with 10 µg/mL chloramphenicol.

429 **Construction of bacterial mutants.** The primers used are listed in Table S4. In-frame
430 deletion of *essC* or *esxC* was performed as described previously (Bae & Schneewind,
431 2006). Briefly, 1-kb DNA fragments up and downstream of the targeted gene sequence
432 were PCR-amplified from USA300 LAC JE2 chromosomal DNA, and both PCR
433 products fused via SOEing (splicing by overlap extension)-PCR. The 2-kb DNA
434 fragment obtained was cloned into pKORI, and used for in-frame deletion. Putative
435 mutants were screened by PCR-amplification of a fragment including the gene of
436 interest, whose deletion was confirmed by Sanger sequencing. Further, to confirm that
437 successful mutants did not have any additional mutations, Illumina whole genome
438 sequencing was performed on libraries prepared with the Nextera XT kit and an
439 Illumina MiSeq® instrument following manufacturers' recommendations. For
440 complementation, full-length *esxC* gene was cloned onto pOS1CK described
441 previously (Korea *et al.*, 2014).

442 **Membrane fluidity assay.** O/N bacterial cultures were diluted to an OD_{600} of 0.15 in
443 TSB, and were grown to an OD_{600} of 1 (OD1). Bacteria were washed with PBS prior
444 to treatment for 30 min at 37ºC with 37.5 µg/mL lysostaphin in PBS containing 20%
445 sucrose. The spheroblasts were then centrifuged at 8000 × *g* for 10 min, and the pellet
446 resuspended in the labelling solution (PBS, 20% sucrose, 0.01% F-127, 5 µM pyrene
447 decanoic acid). The incubation in the dark was done for 1h at 25ºC under gentle
448 rotation. PBS supplemented with 20% sucrose was used to wash the stained

449 spheroblasts that were afterwards transferred to 96-well plates for fluorescence
450 measurements as previously described (Lopez *et al.*, 2017).

451 **Triton X-100 lysis assays.** Whole cell autolysis assays were performed as described
452 elsewhere with a few modifications (Mashruwala *et al.*, 2017). Specifically, OD1-grown
453 *S. aureus* USA300 JE2 WT, *essC* and *esxC* mutants were extensively washed with
454 PBS followed by ice-cold water, and resuspended in PBS with 0.1% Triton X-100 to
455 an OD_{600} of 0.7. Subsequently, the samples were incubated with shaking at 37ºC for
456 2h, after which bacteria were diluted with PBS and plated for CFU determination.

457 **FM1-43 staining.** *S. aureus* WT and mutant strains grown to OD_{600} of 1.0 were
458 centrifuged, and pellets were resuspended in PBS supplemented with 1 µg/mL FM1-
459 43 (Invitrogen). After incubation for 15 min in the dark at 37°C with shaking, cells were
460 washed once with PBS. Fluorescence was quantified using a FLUOstar OMEGA plate
461 reader (BMG Labtech, UK) at excitation and emission wavelengths of 482 nm and 620
462 nm, respectively.

463 **DiIC12 staining.** O/N bacterial cultures were diluted to an OD_{600} of 0.15 in TSB with
464 1 µg/mL 1,1′-didodecyl-3,3,3′,3′-tetramethylindocarbocyanine perchlorate (DiIC12)
465 (Invitrogen). Cultures were grown to an OD_{600} of 1.0, centrifuged and washed twice
466 with fresh TSB. Samples were spotted on to agarose pads and imaged using a Leica
467 DMi8 widefield microscope (Leica Microsystems, UK). Acquired images were
468 analysed with the ImageJ processing package, Fiji.

469 **Growth curves.** O/N bacterial cultures were diluted to an OD_{600} of 0.05 in plain TSB
470 or TSB supplemented with fatty acids. Bacteria were then grown in a 96-well plate with
471 shaking, and the OD_{600} was measured every 15 mins with a FLUOstar OMEGA plate
472 reader (BMG Labtech, UK).

Synthesis of azide functionalized linoleic acid. A 2-step synthesis was used to obtain N^6-diazo-N^2-((9Z,12Z)-octadeca-9,12-dienoyl)lysine, N_3-LA (azide-LA). LA was first functionalized with *N*-hydroxysuccinimide (NHS) in anhydrous dimethyl formamide (DMF) in presence of *N*-(3-dimethylaminopropyl)-*N'*-ethylcarbodiimide hydrochloride. The solvent was then removed and replaced by dicholoromethane (DCM), following which the reaction mixture was washed with water and dried over magnesium sulphate. The product, 2,5-dioxopyrrolidin-1-yl (9Z,12Z)-octadeca-9,12-dienoate (NHS-LA), was analysed using ^{1}H nuclear magnetic resonance (NMR) spectroscopy (Fig. S10A) and mass spectrometry (MS). MS: $[M+Na]^+$ 400.5 (calculated), 400.5 (found).

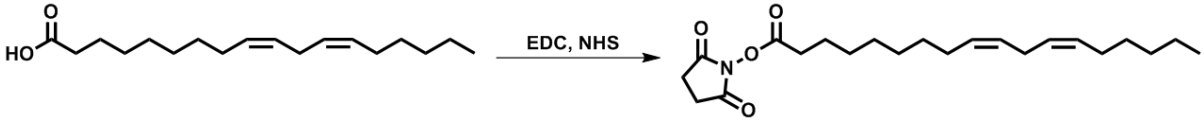

NHS-LA was left O/N at room temperature (RT) to react with L-azidolysine hydrochloride in anhydrous DMF, and produce azide-LA.

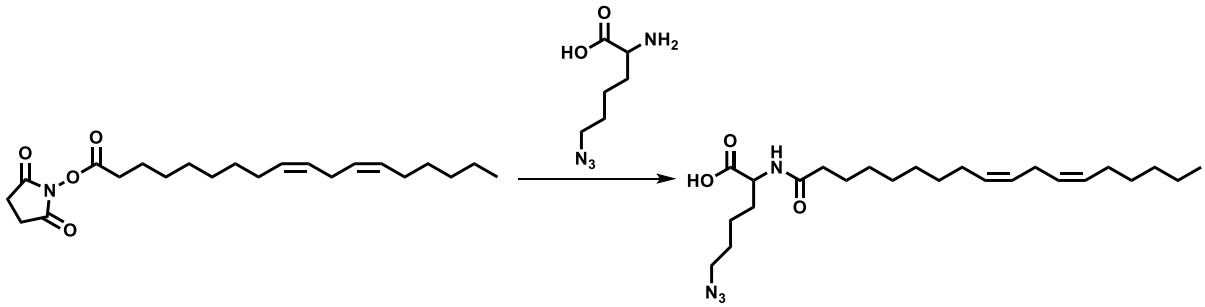

DMF was then removed, the reaction mixture precipitated in water, and dried under vacuum to obtain a clear oil. The composition of the oil was confirmed as being a mixture of azide-LA and unmodified LA (20% and 80%, respectively) based on ^{1}H NMR (Fig. S10B) and MS data. MS: $[LA-H]^-$ 279.5 (calculated), 279.2 (found), $[M-H]^-$ 433.3 (calculated), 433.6 (found).

492 **Binding assays with azide-LA and click chemistry.** *S. aureus* USA300 JE2 WT,
493 Δ*essC*, and Δ*esxC*, grown to OD1, were treated with 10 μM azide-LA for 15 min at
494 37ºC with shaking. The samples were then centrifuged, and the bacterial pellets
495 resuspended in PBS supplemented with 4 μg/mL Click-iT™ Alexa Fluor™ 488 sDIBO
496 alkyne (Life Technologies LTD, UK). After incubation at 25ºC for 1h with shaking,
497 bacteria were washed with PBS, and binding to azide-LA was quantified by measuring
498 fluorescence using a FLUOstar OMEGA plate reader (BMG Labtech, UK). The
499 samples imaged with a microscope were additionally stained with 3 μM propidium
500 iodide, following click chemistry. Bacteria stained with Click-iT™ Alexa Fluor™ 488
501 sDIBO alkyne and 3 μM propidium iodide were immobilized on agarose-covered glass
502 slides, and viewed with a Leica DMi8 widefield microscope (Leica Microsystems LTD,
503 UK). Images were analysed with the ImageJ processing package Fiji (Schindelin *et*
504 *al.*, 2012).

505 **Live/Dead Staining.** Bacteria grown to $OD6_{00}$ of 1.0, were treated with 80 μM linoleic
506 acid for 15 min at 37°C with shaking. The samples were then centrifuged, and the
507 bacterial pellets resuspended in PBS and supplemented with a 1:1 ratio of 2X
508 LIVE/DEAD solution (6 μM SYTO-9 stain and 30 μM propidium iodide) from
509 LIVE/DEAD® BacLight kit (Invitrogen). After incubation in the dark for 15 min, bacteria
510 were washed with PBS, spotted on to agarose pads and imaged using a Leica DMi8
511 widefield microscope (Leica Microsystems, UK). Acquired images were analysed with
512 the ImageJ processing package, Fiji.

513 **Lipid extraction and analyses.** Lipids were extracted from bacterial cultures as
514 described elsewhere (Smith *et al.*, 2019). Briefly, bacteria were grown to OD1 in TSB
515 or TSB supplemented with 10 μM LA, centrifuged in a 2 mL glass Chromacol vial
516 (Thermo Scientific), and resuspended in 0.5 mL MS grade methanol (Sigma-Aldrich).

517 MS grade chloroform was then used to extract lipids. The extracted lipids were dried
518 under nitrogen gas with a Techne sample concentrator (Staffordshire, UK), and the
519 lipid pellets resuspended in 1 mL acetonitrile. The samples were then analysed by LC-
520 MS with a Dionex 3400RS HPLC coupled to an amaZon SL quadrupole ion trap mass
521 spectrometer (Bruker Scientific) via an electrospray ionisation interface. Both positive
522 and negative ionisation modes were used for sample analyses. The Bruker Compass
523 software package was utilized for data analyses, using DataAnalysis for peak
524 identification and characterization of lipid class, and QuantAnalysis for quantification
525 of the relative abundance of distinct PG species to total PG species.

526 **Cell shaving for surface proteome analysis.** *S. aureus* USA300 JE2 WT grown to
527 OD1 and Δ*esxC* were washed three times before being treated with Proteomics grade
528 trypsin from porcine pancreas (Sigma-Aldrich, UK) for 15 min as described (Solis *et*
529 *al.*, 2014). The samples were then centrifuged at 1000 × *g* for 15 min, and the bacterial
530 pellets discarded while supernatants were filtered through a 0.2 μM filter. The freshly
531 prepared peptides were frozen (-20ºC) until 2 additional, independent biological
532 replicates per strain were prepared.

533 **Cellular proteomics.** *S. aureus* strains were grown O/N at 37ºC on tryptic soy agar
534 plates. The next day, single colonies were used to inoculate 10 mL plain TSB or TSB
535 with 10 μM LA. Cultures were grown at 37ºC with 180-rpm shaking until an OD_{600} of
536 3.2 ± 0.2 was reached. The bacteria were then centrifuged, washed with PBS, and
537 resuspended in lysis buffer (PBS, 250 mM sucrose, 1 mM EDTA, and 50 μg/mL
538 lysostaphin) supplemented with cOmplete™, mini, EDTA-free protease inhibitor
539 cocktail (Sigma-Aldrich, UK). After 15 min incubation at 37ºC, cells were lysed
540 mechanically with silica spheres (Lysing Matrix B, Fischer Scientific, UK) in a fast-prep
541 shaker as described previously (Mielich-Suss *et al.*, 2017). Samples were then

542 centrifuged, and the supernatants transferred to fresh tubes, where proteins were
543 reduced and alkylated for 20 min at 70ºC with 10 mM TCEP (tris(2-
544 carboxyethyl)phosphine) and 40 mM CAA (2-chloroacetamide), respectively. Next, the
545 solvent was exchanged first to 8M urea buffer then to 50 mM ammonium bicarbonate
546 (ABC). Proteins were digested O/N at 37ºC with mass spectrometry grade lysyl
547 endopeptidase LysC and sequencing grade modified trypsin (Promega LTD, UK).

548 **Preparation of culture supernatant for proteomics analysis.** *S. aureus* strains
549 were grown to an OD_{600} of 3 in TSB. After centrifugation of cultures, supernatants were
550 sterile-filtered and incubated at 4°C overnight with 10% trichloroacetic acid and 50 µM
551 sodium deoxycholate in presence of one cOmplete™, Mini, EDTA-free Protease
552 Inhibitor Cocktail tablet (Sigma-Aldrich, UK). The precipitated proteins (10 000 × *g* at
553 4ºC for 15 min) were gently washed with acetone and dry at RT for 10 min. After
554 denaturation, proteins were run on a gel until all the proteins had moved from the
555 stacking gel to the resolving gel. The gel was then stained with Instant*Blue*™ (Sigma-
556 Aldrich, UK) for 3 h, after which the protein bands were excised and diced. Proteins
557 were in-gel digested with trypsin as recently described(Goodman *et al.*, 2018). Briefly,
558 proteins were reduced and alkylated for 5 min at 70ºC with 10 mM TCEP and 40 mM
559 CAA, respectively. Tryptic digestion was carried out at O/N at 37°C in 50 mM ABC.

560 **Label-free protein quantification.** Peptides prepared for proteome analyses were
561 desalted and concentrated with a C18 cartridge in 40 µL MS buffer (2% acetonitrile
562 plus 0.1% trifluoroacetic acid). For each sample, 20 µL were analysed by nanoLC-
563 ESI-MS/MS using the Ultimate 3000/Orbitrap Fusion instrumentation (Thermo
564 Scientific), and a 90-minute LC separation on a 50 cm column. The data were used to
565 interrogate the Uniprot *Staphylococcus aureus* USA300 database UP000001939, and
566 the common contaminant database from MaxQuant (Cox *et al.*, 2014). MaxQuant

567 software was used for protein identification and quantification using default settings.
568 Intensities were log_2-tansformed with the Perseus software, and proteins with one or
569 no valid value for every sample in triplicate were filtered. For surfome data, the
570 removeBatchEffect function of the limma R package (Ritchie *et al.*, 2015) was used to
571 remove differences accounting for variation in shaving efficiency done on three
572 different days for all the biological replicates. Missing values in cellular proteomics
573 data were imputed on R. Specifically, for each sample, the imputed value was either
574 the lowest intensity across all samples if at least two biological replicates had missing
575 values or the average of two valid values if only one was missing.

576 **ROS measurement.** Chemical hydrolysis of 2,7-dichlorofluorescein diacetate (Sigma-
577 Aldrich) was performed to acquire a final dichlorofluorescein (DCF) reagent yield of 50
578 µM. Briefly, 0.5 ml of 5 mM DCF-DA (dissolved in 100% ethanol), was reacted with 2
579 ml of 0.1 N NaOH at RT for 30 min. The reaction was stopped using 7.5 mL 10X PBS
580 pH 7.4 (without calcium and magnesium; Gibco). Bacteria grown to OD_{600} of 1.0 were
581 treated with 10µM linoleic acid or left untreated for 15 min at 37°C shaking and 1 mL
582 of this culture was centrifuged. Cells were resuspended in 100 µL of DCF reagent and
583 incubated for 40 min in the dark at RT. Fluorescence was measured using a FLUOstar
584 OMEGA plate reader (BMG Labtech, UK) at an excitation wavelength of 482 nm and
585 emission wavelength of 520 nm.

586 **Data availability statement.** The mass spectrometry proteomics data have been
587 deposited to the ProteomeXchange Consortium via the PRIDE (Perez-Riverol *et al.*,
588 2019) partner repository with the dataset identifier PXD013081 and
589 10.6019/PXD013081. Cellular proteomic and surface proteome samples are labelled
590 MS18-193 and MS17-185, respectively.

591 **Statistical analyses.** Except for the proteomics results, the statistical tests were
592 performed with GraphPad Prism 8.0 as indicated in the Figure legends, with *P* values
593 < 0.05 considered significant. A paired two-tailed Student's t-test or a paired Mann-
594 Whitney U test was used for pairwise comparisons. An ordinary one-way analysis of
595 variance (ANOVA) with Dunnett's multiple comparisons test or a Kruskal-Wallis test
596 with Dunn's multiple comparisons test was applied to data form three or more groups.
597 The fold changes and *P* values of the proteomics data were calculated with the R
598 package limma (Ritchie *et al.*, 2015), with USA300 JE2 WT or bacteria grown without
599 LA as references. These fold changes and *P* values were used by the R package
600 piano (Varemo *et al.*, 2013) to compute the enrichment of gene ontology (GO) terms.

601

602 **Acknowledgments**

603 We thank Professor Tracy Palmer (Newcastle University) and Professor Olaf
604 Scheewind (University of Chicago) for providing us *S. aureus* strains and reagents.
605 We thank GSK, Siena, Italy for providing the *esxA*, *esxB* mutant strains used in this
606 study. We acknowledge the contribution of the Proteomics Research Technology
607 Platform, University of Warwick. The authors have no conflict of interest to declare.

608

609

610

611

612

613

614 **References**

615 Alnaseri, H., Arsic, B., Schneider, J.E., Kaiser, J.C., Scinocca, Z.C., Heinrichs, D.E., and
616 McGavin, M.J. (2015) Inducible Expression of a Resistance-Nodulation-Division-Type
617 Efflux Pump in Staphylococcus aureus Provides Resistance to Linoleic and
618 Arachidonic Acids. *J Bacteriol* **197**: 1893-1905.

619 Aly, K.A., Anderson, M., Ohr, R.J., and Missiakas, D. (2017) Isolation of a Membrane Protein
620 Complex for Type VII Secretion in Staphylococcus aureus. *J Bacteriol* **199**.

621 Anderson, M., Aly, K.A., Chen, Y.H., and Missiakas, D. (2013) Secretion of atypical protein
622 substrates by the ESAT-6 secretion system of Staphylococcus aureus. *Mol Microbiol*
623 **90**: 734-743.

624 Anderson, M., Chen, Y.H., Butler, E.K., and Missiakas, D.M. (2011) EsaD, a secretion factor
625 for the Ess pathway in Staphylococcus aureus. *J Bacteriol* **193**: 1583-1589.

626 Anderson, M., Ohr, R.J., Aly, K.A., Nocadello, S., Kim, H.K., Schneewind, C.E., Schneewind,
627 O., and Missiakas, D. (2017) EssE Promotes Staphylococcus aureus ESS-Dependent
628 Protein Secretion To Modify Host Immune Responses during Infection. *J Bacteriol* **199**.

629 Arsic, B., Zhu, Y., Heinrichs, D.E., and McGavin, M.J. (2012) Induction of the staphylococcal
630 proteolytic cascade by antimicrobial fatty acids in community acquired methicillin
631 resistant Staphylococcus aureus. *PLoS One* **7**: e45952.

632 Bach, J.N., and Bramkamp, M. (2013) Flotillins functionally organize the bacterial membrane.
633 *Mol Microbiol* **88**: 1205-1217.

634 Bae, T., and Schneewind, O. (2006) Allelic replacement in Staphylococcus aureus with
635 inducible counter-selection. *Plasmid* **55**: 58-63.

636 Binns, D., Dimmer, E., Huntley, R., Barrell, D., O'Donovan, C., and Apweiler, R. (2009)
637 QuickGO: a web-based tool for Gene Ontology searching. *Bioinformatics* **25**: 3045-
638 3046.

639 Bobrovskyy, M., Willing, S.E., Schneewind, O., and Missiakas, D. (2018) EssH peptidoglycan
640 hydrolase enables Staphylococcus aureus type VII secretion across the bacterial cell
641 wall envelope. *J Bacteriol*.
642 Burts, M.L., DeDent, A.C., and Missiakas, D.M. (2008) EsaC substrate for the ESAT-6
643 secretion pathway and its role in persistent infections of Staphylococcus aureus. *Mol*
644 *Microbiol* **69**: 736-746.
645 Burts, M.L., Williams, W.A., DeBord, K., and Missiakas, D.M. (2005) EsxA and EsxB are
646 secreted by an ESAT-6-like system that is required for the pathogenesis of
647 Staphylococcus aureus infections. *Proc Natl Acad Sci U S A* **102**: 1169-1174.
648 Cao, Z., Casabona, M.G., Kneuper, H., Chalmers, J.D., and Palmer, T. (2016) The type VII
649 secretion system of Staphylococcus aureus secretes a nuclease toxin that targets
650 competitor bacteria. *Nat Microbiol* **2**: 16183.
651 Cartron, M.L., England, S.R., Chiriac, A.I., Josten, M., Turner, R., Rauter, Y., Hurd, A., Sahl,
652 H.G., Jones, S., and Foster, S.J. (2014) Bactericidal activity of the human skin fatty
653 acid cis-6-hexadecanoic acid on Staphylococcus aureus. *Antimicrob Agents*
654 *Chemother* **58**: 3599-3609.
655 Casabona, M.G., Buchanan, G., Zoltner, M., Harkins, C.P., Holden, M.T.G., and Palmer, T.
656 (2017a) Functional analysis of the EsaB component of the Staphylococcus aureus
657 Type VII secretion system. *Microbiology*.
658 Casabona, M.G., Kneuper, H., Alferes de Lima, D., Harkins, C.P., Zoltner, M., Hjerde, E.,
659 Holden, M.T.G., and Palmer, T. (2017b) Haem-iron plays a key role in the regulation
660 of the Ess/type VII secretion system of Staphylococcus aureus RN6390. *Microbiology*
661 **163**: 1839-1850.
662 Cassat, J., Dunman, P.M., Murphy, E., Projan, S.J., Beenken, K.E., Palm, K.J., Yang, S.J.,
663 Rice, K.C., Bayles, K.W., and Smeltzer, M.S. (2006) Transcriptional profiling of a
664 Staphylococcus aureus clinical isolate and its isogenic agr and sarA mutants reveals
665 global differences in comparison to the laboratory strain RN6390. *Microbiology* **152**:
666 3075-3090.

667 Chamberlain, N.R., Mehrtens, B.G., Xiong, Z., Kapral, F.A., Boardman, J.L., and Rearick, J.I.
668 (1991) Correlation of carotenoid production, decreased membrane fluidity, and
669 resistance to oleic acid killing in Staphylococcus aureus 18Z. *Infect Immun* **59**: 4332-
670 4337.
671 Clarke, S.R., Mohamed, R., Bian, L., Routh, A.F., Kokai-Kun, J.F., Mond, J.J., Tarkowski, A.,
672 and Foster, S.J. (2007) The Staphylococcus aureus surface protein IsdA mediates
673 resistance to innate defenses of human skin. *Cell Host Microbe* **1**: 199-212.
674 Conrad, W.H., Osman, M.M., Shanahan, J.K., Chu, F., Takaki, K.K., Cameron, J., Hopkinson-
675 Woolley, D., Brosch, R., and Ramakrishnan, L. (2017) Mycobacterial ESX-1 secretion
676 system mediates host cell lysis through bacterium contact-dependent gross membrane
677 disruptions. *Proc Natl Acad Sci U S A* **114**: 1371-1376.
678 Cox, J., Hein, M.Y., Luber, C.A., Paron, I., Nagaraj, N., and Mann, M. (2014) Accurate
679 proteome-wide label-free quantification by delayed normalization and maximal peptide
680 ratio extraction, termed MaxLFQ. *Mol Cell Proteomics* **13**: 2513-2526.
681 Cruciani, M., Etna, M.P., Camilli, R., Giacomini, E., Percario, Z.A., Severa, M., Sandini, S.,
682 Rizzo, F., Brandi, V., Balsamo, G., Polticelli, F., Affabris, E., Pantosti, A., Bagnoli, F.,
683 and Coccia, E.M. (2017) Staphylococcus aureus Esx Factors Control Human Dendritic
684 Cell Functions Conditioning Th1/Th17 Response. *Front Cell Infect Microbiol* **7**: 330.
685 Delekta, P.C., Shook, J.C., Lydic, T.A., Mulks, M.H., and Hammer, N.D. (2018)
686 Staphylococcus aureus utilizes host-derived lipoprotein particles as sources of
687 exogenous fatty acids. *J Bacteriol*.
688 Dreisbach, A., Hempel, K., Buist, G., Hecker, M., Becher, D., and van Dijl, J.M. (2010) Profiling
689 the surfacome of Staphylococcus aureus. *Proteomics* **10**: 3082-3096.
690 Fey, P.D., Endres, J.L., Yajjala, V.K., Widhelm, T.J., Boissy, R.J., Bose, J.L., and Bayles, K.W.
691 (2013) A genetic resource for rapid and comprehensive phenotype screening of
692 nonessential Staphylococcus aureus genes. *MBio* **4**: e00537-00512.
693 Garcia-Fernandez, E., Koch, G., Wagner, R.M., Fekete, A., Stengel, S.T., Schneider, J.,
694 Mielich-Suss, B., Geibel, S., Markert, S.M., Stigloher, C., and Lopez, D. (2017)

695 Membrane Microdomain Disassembly Inhibits MRSA Antibiotic Resistance. *Cell* **171**:
696 1354-1367 e1320.
697 Geiger, T., Francois, P., Liebeke, M., Fraunholz, M., Goerke, C., Krismer, B., Schrenzel, J.,
698 Lalk, M., and Wolz, C. (2012) The stringent response of Staphylococcus aureus and
699 its impact on survival after phagocytosis through the induction of intracellular PSMs
700 expression. *PLoS Pathog* **8**: e1003016.
701 George, S.E., Hrubesch, J., Breuing, I., Vetter, N., Korn, N., Hennemann, K., Bleul, L.,
702 Willmann, M., Ebner, P., Gotz, F., and Wolz, C. (2019) Oxidative stress drives the
703 selection of quorum sensing mutants in the Staphylococcus aureus population. *Proc*
704 *Natl Acad Sci U S A* **116**: 19145-19154.
705 Giachino, P., Engelmann, S., and Bischoff, M. (2001) Sigma(B) activity depends on RsbU in
706 Staphylococcus aureus. *J Bacteriol* **183**: 1843-1852.
707 Goodman, J.K., Zampronio, C.G., Jones, A.M.E., and Hernandez-Fernaud, J.R. (2018)
708 Updates of the In-Gel Digestion Method for Protein Analysis by Mass Spectrometry.
709 *Proteomics* **18**: e1800236.
710 Gordon, R.J., and Lowy, F.D. (2008) Pathogenesis of methicillin-resistant Staphylococcus
711 aureus infection. *Clin Infect Dis* **46 Suppl 5**: S350-359.
712 Greenway, D.L., and Dyke, K.G. (1979) Mechanism of the inhibitory action of linoleic acid on
713 the growth of Staphylococcus aureus. *J Gen Microbiol* **115**: 233-245.
714 Groicher, K.H., Firek, B.A., Fujimoto, D.F., and Bayles, K.W. (2000) The Staphylococcus
715 aureus lrgAB operon modulates murein hydrolase activity and penicillin tolerance. *J*
716 *Bacteriol* **182**: 1794-1801.
717 Hempel, K., Herbst, F.A., Moche, M., Hecker, M., and Becher, D. (2011) Quantitative
718 proteomic view on secreted, cell surface-associated, and cytoplasmic proteins of the
719 methicillin-resistant human pathogen Staphylococcus aureus under iron-limited
720 conditions. *J Proteome Res* **10**: 1657-1666.
721 Horsburgh, M.J., Ingham, E., and Foster, S.J. (2001) In Staphylococcus aureus, fur is an
722 interactive regulator with PerR, contributes to virulence, and Is necessary for oxidative

723 stress resistance through positive regulation of catalase and iron homeostasis. *J*
724 *Bacteriol* **183**: 468-475.
725 Ishii, K., Adachi, T., Yasukawa, J., Suzuki, Y., Hamamoto, H., and Sekimizu, K. (2014)
726 Induction of virulence gene expression in Staphylococcus aureus by pulmonary
727 surfactant. *Infect Immun* **82**: 1500-1510.
728 Jager, F., Kneuper, H., and Palmer, T. (2018) EssC is a specificity determinant for
729 Staphylococcus aureus type VII secretion. *Microbiology* **164**: 816-820.
730 Johnson, M., Sengupta, M., Purves, J., Tarrant, E., Williams, P.H., Cockayne, A., Muthaiyan,
731 A., Stephenson, R., Ledala, N., Wilkinson, B.J., Jayaswal, R.K., and Morrissey, J.A.
732 (2011) Fur is required for the activation of virulence gene expression through the
733 induction of the sae regulatory system in Staphylococcus aureus. *Int J Med Microbiol*
734 **301**: 44-52.
735 Kelsey, J.A., Bayles, K.W., Shafii, B., and McGuire, M.A. (2006) Fatty acids and
736 monoacylglycerols inhibit growth of Staphylococcus aureus. *Lipids* **41**: 951-961.
737 Kenny, J.G., Ward, D., Josefsson, E., Jonsson, I.M., Hinds, J., Rees, H.H., Lindsay, J.A.,
738 Tarkowski, A., and Horsburgh, M.J. (2009) The Staphylococcus aureus response to
739 unsaturated long chain free fatty acids: survival mechanisms and virulence
740 implications. *PLoS One* **4**: e4344.
741 Kneuper, H., Cao, Z.P., Twomey, K.B., Zoltner, M., Jager, F., Cargill, J.S., Chalmers, J., van
742 der Kooi-Pol, M.M., van Dijl, J.M., Ryan, R.P., Hunter, W.N., and Palmer, T. (2014)
743 Heterogeneity in ess transcriptional organization and variable contribution of the
744 Ess/Type VII protein secretion system to virulence across closely related
745 Staphylocccus aureus strains. *Mol Microbiol* **93**: 928-943.
746 Kohler, T., Weidenmaier, C., and Peschel, A. (2009) Wall teichoic acid protects
747 Staphylococcus aureus against antimicrobial fatty acids from human skin. *J Bacteriol*
748 **191**: 4482-4484.
749 Korea, C.G., Balsamo, G., Pezzicoli, A., Merakou, C., Tavarini, S., Bagnoli, F., Serruto, D.,
750 and Unnikrishnan, M. (2014) Staphylococcal Esx proteins modulate apoptosis and

751 release of intracellular Staphylococcus aureus during infection in epithelial cells. *Infect*
752 *Immun* **82**: 4144-4153.
753 Lee, A.S., de Lencastre, H., Garau, J., Kluytmans, J., Malhotra-Kumar, S., Peschel, A., and
754 Harbarth, S. (2018) Methicillin-resistant Staphylococcus aureus. *Nat Rev Dis Primers*
755 **4**: 18033.
756 Liang, X., Zheng, L., Landwehr, C., Lunsford, D., Holmes, D., and Ji, Y. (2005) Global
757 regulation of gene expression by ArlRS, a two-component signal transduction
758 regulatory system of Staphylococcus aureus. *J Bacteriol* **187**: 5486-5492.
759 Lopez, M.S., Tan, I.S., Yan, D., Kang, J., McCreary, M., Modrusan, Z., Austin, C.D., Xu, M.,
760 and Brown, E.J. (2017) Host-derived fatty acids activate type VII secretion in
761 Staphylococcus aureus. *Proc Natl Acad Sci U S A* **114**: 11223-11228.
762 Mashruwala, A.A., Guchte, A.V., and Boyd, J.M. (2017) Impaired respiration elicits SrrAB-
763 dependent programmed cell lysis and biofilm formation in Staphylococcus aureus. *Elife*
764 **6**.
765 Mielich-Suss, B., Wagner, R.M., Mietrach, N., Hertlein, T., Marincola, G., Ohlsen, K., Geibel,
766 S., and Lopez, D. (2017) Flotillin scaffold activity contributes to type VII secretion
767 system assembly in Staphylococcus aureus. *PLoS Pathog* **13**: e1006728.
768 Moran, J.C., Alorabi, J.A., and Horsburgh, M.J. (2017) Comparative Transcriptomics Reveals
769 Discrete Survival Responses of S. aureus and S. epidermidis to Sapienic Acid. *Front*
770 *Microbiol* **8**: 33.
771 Neumann, Y., Ohlsen, K., Donat, S., Engelmann, S., Kusch, H., Albrecht, D., Cartron, M.,
772 Hurd, A., and Foster, S.J. (2015) The effect of skin fatty acids on Staphylococcus
773 aureus. *Arch Microbiol* **197**: 245-267.
774 Nguyen, M.T., Hanzelmann, D., Hartner, T., Peschel, A., and Gotz, F. (2016) Skin-Specific
775 Unsaturated Fatty Acids Boost the Staphylococcus aureus Innate Immune Response.
776 *Infect Immun* **84**: 205-215.
777 Ohr, R.J., Anderson, M., Shi, M., Schneewind, O., and Missiakas, D. (2017) EssD, a Nuclease
778 Effector of the Staphylococcus aureus ESS Pathway. *J Bacteriol* **199**.

779 Parsons, J.B., Broussard, T.C., Bose, J.L., Rosch, J.W., Jackson, P., Subramanian, C., and
780 Rock, C.O. (2014) Identification of a two-component fatty acid kinase responsible for
781 host fatty acid incorporation by Staphylococcus aureus. *Proc Natl Acad Sci U S A* **111**:
782 10532-10537.
783 Parsons, J.B., Frank, M.W., Subramanian, C., Saenkham, P., and Rock, C.O. (2011)
784 Metabolic basis for the differential susceptibility of Gram-positive pathogens to fatty
785 acid synthesis inhibitors. *Proc Natl Acad Sci U S A* **108**: 15378-15383.
786 Parsons, J.B., Yao, J., Frank, M.W., Jackson, P., and Rock, C.O. (2012) Membrane disruption
787 by antimicrobial fatty acids releases low-molecular-weight proteins from
788 Staphylococcus aureus. *J Bacteriol* **194**: 5294-5304.
789 Pasztor, L., Ziebandt, A.K., Nega, M., Schlag, M., Haase, S., Franz-Wachtel, M., Madlung, J.,
790 Nordheim, A., Heinrichs, D.E., and Gotz, F. (2010) Staphylococcal major autolysin (Atl)
791 is involved in excretion of cytoplasmic proteins. *J Biol Chem* **285**: 36794-36803.
792 Patton, T.G., Yang, S.J., and Bayles, K.W. (2006) The role of proton motive force in expression
793 of the Staphylococcus aureus cid and lrg operons. *Mol Microbiol* **59**: 1395-1404.
794 Perez-Riverol, Y., Csordas, A., Bai, J., Bernal-Llinares, M., Hewapathirana, S., Kundu, D.J.,
795 Inuganti, A., Griss, J., Mayer, G., Eisenacher, M., Perez, E., Uszkoreit, J., Pfeuffer, J.,
796 Sachsenberg, T., Yilmaz, S., Tiwary, S., Cox, J., Audain, E., Walzer, M., Jarnuczak,
797 A.F., Ternent, T., Brazma, A., and Vizcaino, J.A. (2019) The PRIDE database and
798 related tools and resources in 2019: improving support for quantification data. *Nucleic*
799 *Acids Res* **47**: D442-D450.
800 Pulschen, A.A., Sastre, D.E., Machinandiarena, F., Crotta Asis, A., Albanesi, D., de Mendoza,
801 D., and Gueiros-Filho, F.J. (2017) The stringent response plays a key role in Bacillus
802 subtilis survival of fatty acid starvation. *Mol Microbiol* **103**: 698-712.
803 Ritchie, M.E., Phipson, B., Wu, D., Hu, Y., Law, C.W., Shi, W., and Smyth, G.K. (2015) limma
804 powers differential expression analyses for RNA-sequencing and microarray studies.
805 *Nucleic Acids Res* **43**: e47.

806 Saeloh, D., Tipmanee, V., Jim, K.K., Dekker, M.P., Bitter, W., Voravuthikunchai, S.P., Wenzel,
807 M., and Hamoen, L.W. (2018) The novel antibiotic rhodomyrtone traps membrane
808 proteins in vesicles with increased fluidity. *PLoS Pathog* **14**: e1006876.
809 Schindelin, J., Arganda-Carreras, I., Frise, E., Kaynig, V., Longair, M., Pietzsch, T., Preibisch,
810 S., Rueden, C., Saalfeld, S., Schmid, B., Tinevez, J.Y., White, D.J., Hartenstein, V.,
811 Eliceiri, K., Tomancak, P., and Cardona, A. (2012) Fiji: an open-source platform for
812 biological-image analysis. *Nat Methods* **9**: 676-682.
813 Sen, S., Sirobhushanam, S., Johnson, S.R., Song, Y., Tefft, R., Gatto, C., and Wilkinson, B.J.
814 (2016) Growth-Environment Dependent Modulation of Staphylococcus aureus
815 Branched-Chain to Straight-Chain Fatty Acid Ratio and Incorporation of Unsaturated
816 Fatty Acids. *PLoS One* **11**: e0165300.
817 Smith, A.F., Rihtman, B., Stirrup, R., Silvano, E., Mausz, M.A., Scanlan, D.J., and Chen, Y.
818 (2019) Elucidation of glutamine lipid biosynthesis in marine bacteria reveals its
819 importance under phosphorus deplete growth in Rhodobacteraceae. *ISME J* **13**: 39-
820 49.
821 Solis, N., Parker, B.L., Kwong, S.M., Robinson, G., Firth, N., and Cordwell, S.J. (2014)
822 Staphylococcus aureus surface proteins involved in adaptation to oxacillin identified
823 using a novel cell shaving approach. *J Proteome Res* **13**: 2954-2972.
824 Tiwari, K.B., Gatto, C., and Wilkinson, B.J. (2018) Interrelationships between Fatty Acid
825 Composition, Staphyloxanthin Content, Fluidity, and Carbon Flow in the
826 Staphylococcus aureus Membrane. *Molecules* **23**.
827 Tong, S.Y., Davis, J.S., Eichenberger, E., Holland, T.L., and Fowler, V.G., Jr. (2015)
828 Staphylococcus aureus infections: epidemiology, pathophysiology, clinical
829 manifestations, and management. *Clin Microbiol Rev* **28**: 603-661.
830 Truong-Bolduc, Q.C., Villet, R.A., Estabrooks, Z.A., and Hooper, D.C. (2014) Native efflux
831 pumps contribute resistance to antimicrobials of skin and the ability of Staphylococcus
832 aureus to colonize skin. *J Infect Dis* **209**: 1485-1493.

833 Unnikrishnan, M., Constantinidou, C., Palmer, T., and Pallen, M.J. (2017) The Enigmatic Esx
834 Proteins: Looking Beyond Mycobacteria. *Trends Microbiol* **25**: 192-204.
835 Varemo, L., Nielsen, J., and Nookaew, I. (2013) Enriching the gene set analysis of genome-
836 wide data by incorporating directionality of gene expression and combining statistical
837 hypotheses and methods. *Nucleic Acids Res* **41**: 4378-4391.
838 Ventura, C.L., Malachowa, N., Hammer, C.H., Nardone, G.A., Robinson, M.A., Kobayashi,
839 S.D., and DeLeo, F.R. (2010) Identification of a novel Staphylococcus aureus two-
840 component leukotoxin using cell surface proteomics. *PLoS One* **5**: e11634.
841 von Eiff, C., Becker, K., Machka, K., Stammer, H., and Peters, G. (2001) Nasal carriage as a
842 source of Staphylococcus aureus bacteremia. Study Group. *N Engl J Med* **344**: 11-16.
843 Wang, Y., Hu, M., Liu, Q., Qin, J., Dai, Y., He, L., Li, T., Zheng, B., Zhou, F., Yu, K., Fang, J.,
844 Liu, X., Otto, M., and Li, M. (2016) Role of the ESAT-6 secretion system in virulence
845 of the emerging community-associated Staphylococcus aureus lineage ST398. *Sci*
846 *Rep* **6**: 25163.
847 Warne, B., Harkins, C.P., Harris, S.R., Vatsiou, A., Stanley-Wall, N., Parkhill, J., Peacock,
848 S.J., Palmer, T., and Holden, M.T. (2016) The Ess/Type VII secretion system of
849 Staphylococcus aureus shows unexpected genetic diversity. *BMC Genomics* **17**: 222.
850 Wood, T.E., Howard, S.A., Forster, A., Nolan, L.M., Manoli, E., Bullen, N.P., Yau, H.C.L.,
851 Hachani, A., Hayward, R.D., Whitney, J.C., Vollmer, W., Freemont, P.S., and Filloux,
852 A. (2019) The Pseudomonas aeruginosa T6SS Delivers a Periplasmic Toxin that
853 Disrupts Bacterial Cell Morphology. *Cell Rep* **29**: 187-201 e187.
854 Zoltner, M., Ng, W.M., Money, J.J., Fyfe, P.K., Kneuper, H., Palmer, T., and Hunter, W.N.
855 (2016) EssC: domain structures inform on the elusive translocation channel in the Type
856 VII secretion system. *Biochem J* **473**: 1941-1952.

857

858 **Figure legends**

859 **Fig. 1. Membrane defects in the absence of EsxC.**

860 **A**. FM1-43 fluorescence of *S. aureus* WT, Δ*essC*, and Δ*esxC* as measured with a
861 plate reader. Means ± standard deviation (SD) are shown, $n = 6$; * indicates $P < 0.05$
862 using a Kruskal-Wallis test with Dunn's test.

863 **B**. Survival of Δ*esxC* or Δ*essC* after a 2h-treatment with 0.1% Triton X-100 relative to
864 the WT. Means are shown; error bars represent standard deviation (SD). $n = 4$, *
865 indicates $P < 0.05$ using a Kruskal-Wallis test with Dunn's test. The panel on the right
866 shows a representative picture of bacteria before and after Triton X-100-treatment.

867 **C**. The membrane fluidity of WT and Δ*esxC* as measured with a pyrene decanoic acid
868 staining-based assay. Mean values are shown; error bars represent standard error of
869 the mean (SEM). $n = 6$, * indicates $P < 0.05$ using a two-tailed t-test.

870 **D**. Widefield micrographs of *S. aureus* WT and Δ*esxC* after growth in TSB to OD_{600} of
871 1.0 in the presence of the lipophilic dye DiIC12. Images are representative of 4
872 independent experiments.

873 **E**. The DiIC12 fluorescence of 80 bacterial clusters from different fields per strain was
874 quantitated with ImageJ. Means ± standard deviation (SD) are shown, $n = 4$; indicates
875 **** $P < 0.0001$, using a Kruskal-Wallis rank test

876 **Fig. 2. Enhanced *S. aureus* growth inhibition by linoleic acid in T7SS mutants.**

877 **A**. *S. aureus* WT USA300, Δ*essC*, and Δ*esxC* were grown in TSB or TSB
878 supplemented with 80 μM of either linoleic (LA) or stearic acid (SA). Means ± standard
879 error of the mean (SEM) are shown.

880 **B**. After 14h growth as described in (A) bacteria were serially diluted, and CFU were
881 determined. Mean values are presented, and the error bars represent SD. n = 3, **
882 indicates $P < 0.01$ using one-way ANOVA with Dunnett's test.
883 **C**. USA300 WT with the empty pOS1 plasmid (WT pOS1) and USA300 JE2 *esxC*
884 mutant with either pOS1 (Δ*esxC* pOS1) or pOS1-*esxC* (Δ*esxC* pOS1-*esxC*) were
885 grown in TSB or TSB + 80 μM LA as described in (A) followed by CFU estimation.
886 Mean values are shown; error bars represent SD. n = 5, ** indicates $P < 0.01$ using
887 one-way ANOVA with Dunnett's test.
888 **D**. Newman WT with the empty pOS1 plasmid (WT pOS1) and Newman *esxA* mutant
889 with either pOS1 (Δ*esxA* pOS1) or pOS1-*esxA* (Δ*esxA* p*esxA*) were grown in TSB or
890 TSB + 40 μM LA or SA. Means ± standard error of the mean (SEM) are shown, n = 4**.**

891 **Fig. 3. T7SS mutants display increased membrane permeability upon LA**
892 **binding.**
893 **A**. Chemical structure of azide functionalised linoleic acid (azide-LA; N^6-diazo-N^2-
894 ((9Z,12Z)-octadeca-9,12-dienoyl)lysine, N_3-LA). Highlighted in green is the azido
895 lysine.
896 **B**. *S. aureus* USA300 WT, Δ*essC*, and Δ*esxC* were grown with shaking in TSB to
897 OD_{600} of 1.0. Bacteria were then stained for 15 min with 10 μM azide-LA prior to
898 labelling for 1 h with alkyne Alexa Fluor 488. Mean percentage of fluorescence values
899 relative to WT (100%) are presented; error bars represent SD, n = 5.
900 **C**. Micrographs of bacteria grown in TSB and treated as described in (B) and
901 additionally stained with propidium iodide (PI).
902 **D**. ImageJ was used to quantitate PI fluorescence of bacterial clusters from 12 different
903 fields per strain. Each box-and-whisker plot depicts the minimal and maximal PI

904 intensities, the median is the vertical bar inside the box, which is delimited by the lower
905 and upper quartiles. ** indicates $P < 0.01$ using one-way ANOVA with Dunnett's test.

906 **Fig. 4. T7SS mutants display increased PI staining when treated with LA.**
907 Live/Dead staining of *S. aureus* USA300 WT, Δ*essC* or Δ*esxC* mutants after growth
908 to OD_{600} of 1.0, without (**A**) or with treatment with 80μM (**B**) linoleic acid. Images are
909 representative of 3 independent experiments.
910 **C**. The ratio of SYTO 9: PI fluorescence (live:dead cells) of 25 different fields per strain
911 was quantitated with ImageJ. Means ± SD are shown, $n = 3$; *** indicates $P < 0.001$,
912 ** indicates $P < 0.01$ using a one-way ANOVA with Tukey's multiple-comparison test

913 **Fig. 5. T7SS mutants are less able to incorporate LA into their phospholipids.**
914 Representative HPLC chromatograms of native phosphatidylglycerol (PG) species of
915 *S. aureus* USA300 JE2 WT (**A**) or Δ*esxC* (**B**) grown in TSB (top panel) or in TSB
916 supplemented with 10 μM LA (bottom panel), in negative ionisation mode. Relative
917 quantification of the indicated PG species containing an unsaturated FA in WT, Δ*essC*
918 and Δ*esxC*. C18:2-containing PG species (**C**) and total unsaturated exogenous PG
919 species (**D**) are presented as ratios of total PG species. Mean values are shown; error
920 bars represent SD. $n = 3$, * indicates $P < 0.05$ using one-way ANOVA with Dunnett's
921 test.

922 **Fig. 6. Quantitative proteomics shows altered cellular content and bacterial**
923 **response to LA in T7SS mutants.** *S. aureus* USA300 WT and mutants (Δ*essC* and
924 Δ*esxC*) were grown in TSB or TSB supplemented with LA.
925 **A**. Venn diagram showing the number of proteins with altered abundance compared
926 to WT specific to Δ*essC* (23) or Δ*esxC* (10), and common to Δ*essC* and Δ*esxC* (14).

927 **B**. The fourteen proteins that are similarly changed in Δ*essC* and Δ*esxC* mutants are
928 highlighted on a volcano plot.
929 **C**. Volcano plot showing the extensive change in the LA-treated WT compared to WT.
930 **D**. Venn diagram displaying the numbers of proteins with altered relative abundance
931 upon LA challenge of WT (LA.WT), Δ*essC* (LA.dEssC) or Δ*esxC* (LA.dEsxC)
932 compared to the respective untreated samples.

933 **Fig. 7. An altered oxidoreductive response in T7SS mutants in response to LA.**
934 Heatmaps depicting the *P* values of enriched (**A**) or diminished (**B**) molecular functions
935 following a gene set analysis based on GO (gene ontology) annotations. Molecular
936 functions that are changed in at least one strain ($P < 0.05$) following growth in presence
937 of LA are shown. The shades of blue (**A**) or red (**B**) correspond to $-\log_{10}$ (*P* value).
938 ROS levels were measured in cultures of *S. aureus* USA300 JE2 WT, Δ*essC* or Δ*esxC*
939 grown to OD_{600} of 1.0 treated (**C)** with or without LA (**D**) using DCF reagent. Means ±
940 SD are shown N=5. * indicates $P < 0.05$, ** indicates $P < 0.01$, *** indicates $P < 0.001$
941 using the Kruskal-Wallis rank test.

942 **Fig. S1. USA300 JE2 WT and Δ*esxC* strains display similar growth rates.** WT and
943 Δ*esxC* were grown in TSB, and OD_{600} monitored with a Novaspec® Pro
944 spectrophotometer. Data shown are means of three independent experiments, and
945 the error bars indicate the standard errors of the mean.

946 **Fig. S2. EsxC associates with *S. aureus* membrane**. Immunoblot analysis of cell
947 membrane (CM) or cell wall (CW) fractions of WT (USA300), Δ*essC*, and Δ*esxC* with
948 anti-EsxC sera or anti-PBP2a antibodies (loading control).

949 **Fig. S3. Volcano plot of the quantitative proteomic analysis of surface proteins**
950 **in Δ*esxC* compared to WT.** The relative abundance of each protein ($\log_2$ fold change,

951 X-axis) and its statistical significance (*P* value, Y-axis) are shown in the graph.
952 Proteins decreased by more than half in Δ*esxC* (log_2 fold change < -1 and *P* value <
953 0.05) are shown in green.

954 **Fig. S4. *S. aureus* growth inhibition by arachidonic acid is increased in T7SS**
955 **mutants.** *S. aureus* WT USA300, Δ*essC*, and Δ*esxC* were grown in TSB or TSB
956 supplemented with 80 μM arachidonic acid (AA). Means ± standard error of the mean
957 (SEM) are shown, *n* = 3.

958 **Fig. S5. T7SS substrates contribute to resistance to linoleic acid toxicity**.
959 A. *S. aureus* USA300 wild-type (WT) and USA300 *esxA* (Δ*esxA*) or *esxB* (Δ*esxB*)
960 deletion mutants were grown in TSB or TSB supplemented with 80 μM linoleic (LA) or
961 stearic acid (SA).
962 B. *S. aureus* Newman WT and Newman *esxA* (Δ*esxA*) or *esxB* (Δ*esxB*) deletion
963 mutants were grown similarly in TSB or TSB + 40 μM LA or SA.
964 C. Growth curves as described in (A) were done with RN6390 wild-type (WT) and
965 RN6390 *essC* (Δ*essC*) or *esxC* (Δ*esxC*) deletion mutants. Data shown in (A), (B), and
966 (C) are representative of at least three independent experiments.

967 **Fig. S6. USA300 JE2 WT and T7SS mutants display similar lipids.**
968 Representative HPLC chromatograms of the indicated bacteria grown in TSB (A) or in
969 TSB supplemented with LA (B), in negative ionisation mode. Phosphatidylglycerol
970 (PG) is highlighted.
971 C. Representative HPLC chromatograms of native PG species of Δ*essC* grown in TSB
972 (top panel) or in TSB supplemented with LA (bottom panel), in negative ionisation
973 mode.

974 **Fig. S7. LA (C18:2) is elongated and incorporated into *S. aureus***
975 **phosphatidylglycerol (PG) species.** A-C. Representative mass spectrometry
976 fragmentation spectra for PG species containing unsaturated fatty acids, in negative
977 ionisation mode.
978 A. PG species with mass 731 m/z, containing C18:2 fatty acid (279 m/z).
979 B. PG species 759 m/z, containing C20:2 fatty acid (307 m/z)
980 C. PG species 787 m/z, containing C22:2 fatty acid (335 m/z).
981 D. and E. Relative quantification of the indicated PG species containing an
982 unsaturated fatty acid in WT, Δ*essC* and Δ*esxC*. C20:2- (D) and C22:2-containing PG
983 species (E) are presented as ratios of total PG species. Data shown are the means
984 and error bars represent SD of three independent experiments.

985 **Fig. S8. USA300 JE2 WT and Δ*esxC* growth similarly in presence of sub-**
986 **inhibitory amounts of linoleic acid.** *S. aureus* WT USA300 and Δ*esxC* were grown
987 in TSB or TSB supplemented with 40 μM linoleic acid (LA). Means ± SEM are shown,
988 n = 3.

989 **Fig. S9. Principal component analysis (PCA) of the *S. aureus* cellular proteomic**
990 **profiles.** PCA was performed on all the identified proteins of USA300 JE2 WT and
991 T7SS mutants grown in TSB (untreated) or TSB + LA (LA-treated). Each dot
992 represents a biological replicate.

993 **Fig. S10. ^{1}H NMR spectra of NHS-LA (A) and azide-LA (B) in $CDCl_3$.** Both spectra
994 were recorded on a Bruker Advance 300 spectrometer (300 MHz) at 27 °C. The letters
995 indicate the chemical shift δ (in parts per million, ppm) of the protons in each molecule.

996 **Dataset S1. Differentially abundant proteins in WT USA300 JE2 and T7SS**
997 **mutants in response to linoleic acid**.

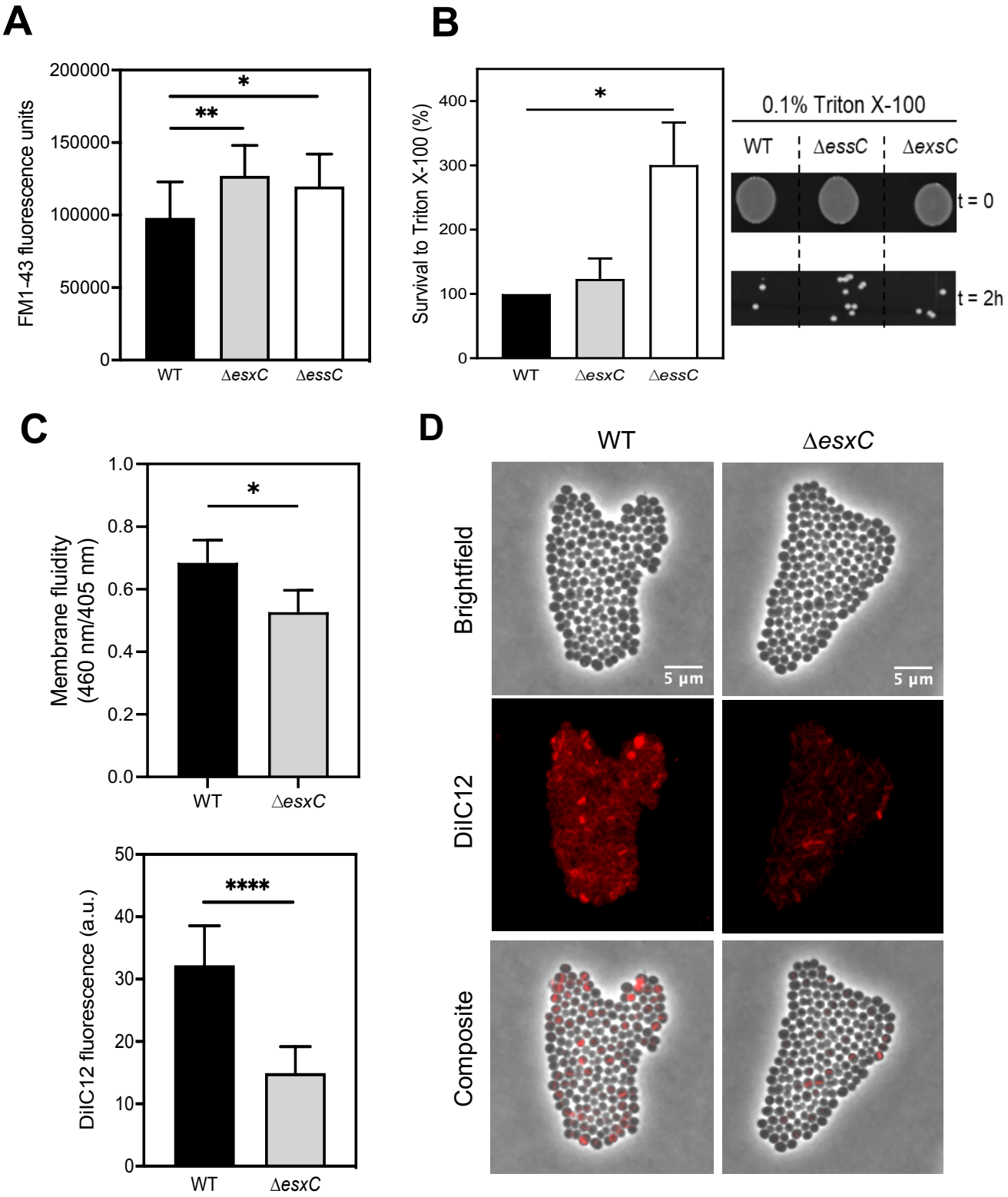
A
FM1-43 fluorescence units
200000
150000
100000
50000
0
*
**
WT
ΔesxC
ΔessC
B
Survival to Triton X-100 (%)
400
300
200
100
0
*
WT
ΔesxC
ΔessC
0.1% Triton X-100
WT
ΔessC
ΔexsC
t = 0
t = 2h
C
Membrane fluidity
(460 nm/405 nm)
1.0
0.8
0.6
0.4
0.2
0.0
*
WT
ΔesxC
DiIC12 fluorescence (a.u.)
50
40
30
20
10
0
****
WT
ΔesxC
D
WT
ΔesxC
Brightfield
DiIC12
Composite
5 µm
5 µm

Fig 1

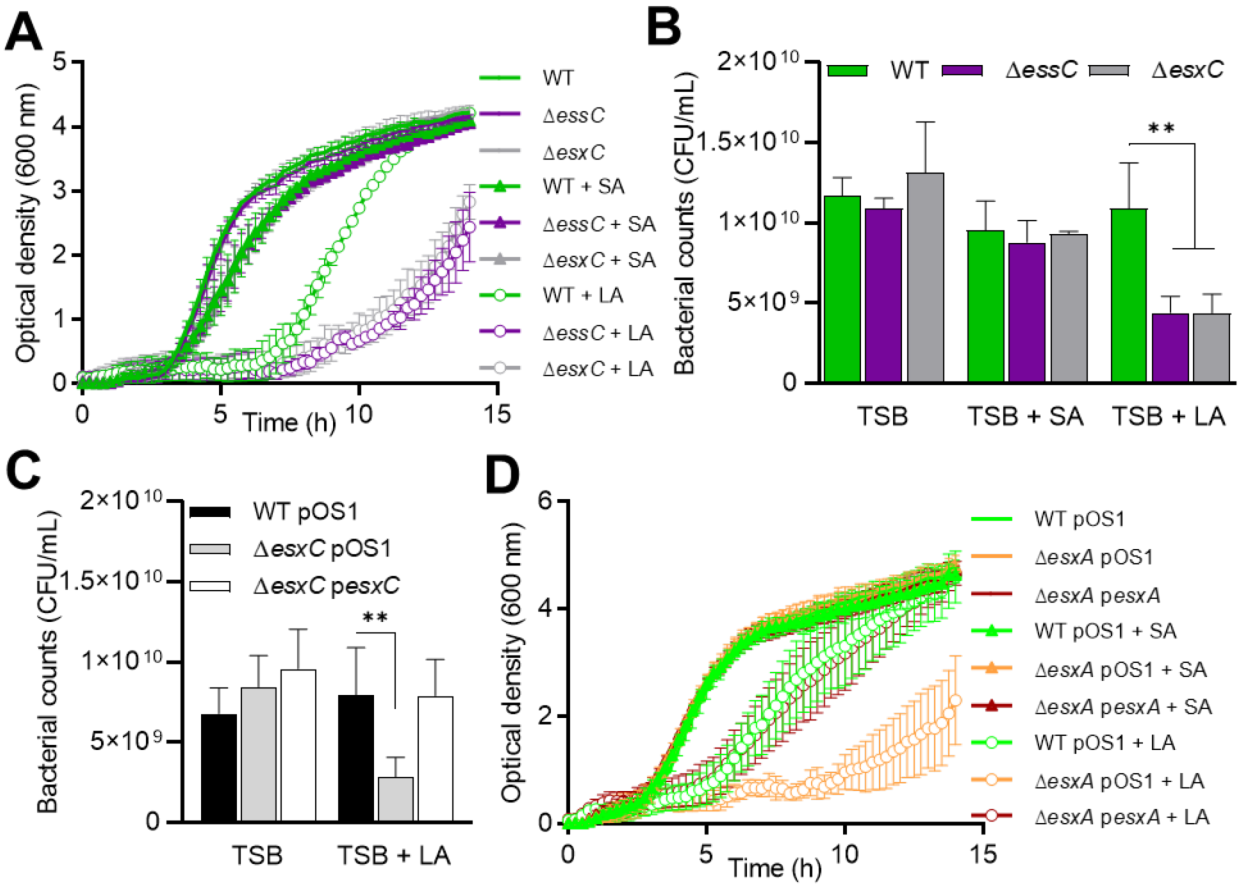
A
Optical density (600 nm)
Time (h)
WT
ΔessC
ΔesxC
WT + SA
ΔessC + SA
ΔesxC + SA
WT + LA
ΔessC + LA
ΔesxC + LA
B
Bacterial counts (CFU/mL)
WT
ΔessC
ΔesxC
**
TSB
TSB + SA
TSB + LA
C
Bacterial counts (CFU/mL)
WT pOS1
ΔesxC pOS1
ΔesxC pesxC
**
TSB
TSB + LA
D
Optical density (600 nm)
Time (h)
WT pOS1
ΔesxA pOS1
ΔesxA pesxA
WT pOS1 + SA
ΔesxA pOS1 + SA
ΔesxA pesxA + SA
WT pOS1 + LA
ΔesxA pOS1 + LA
ΔesxA pesxA + LA

Fig 2

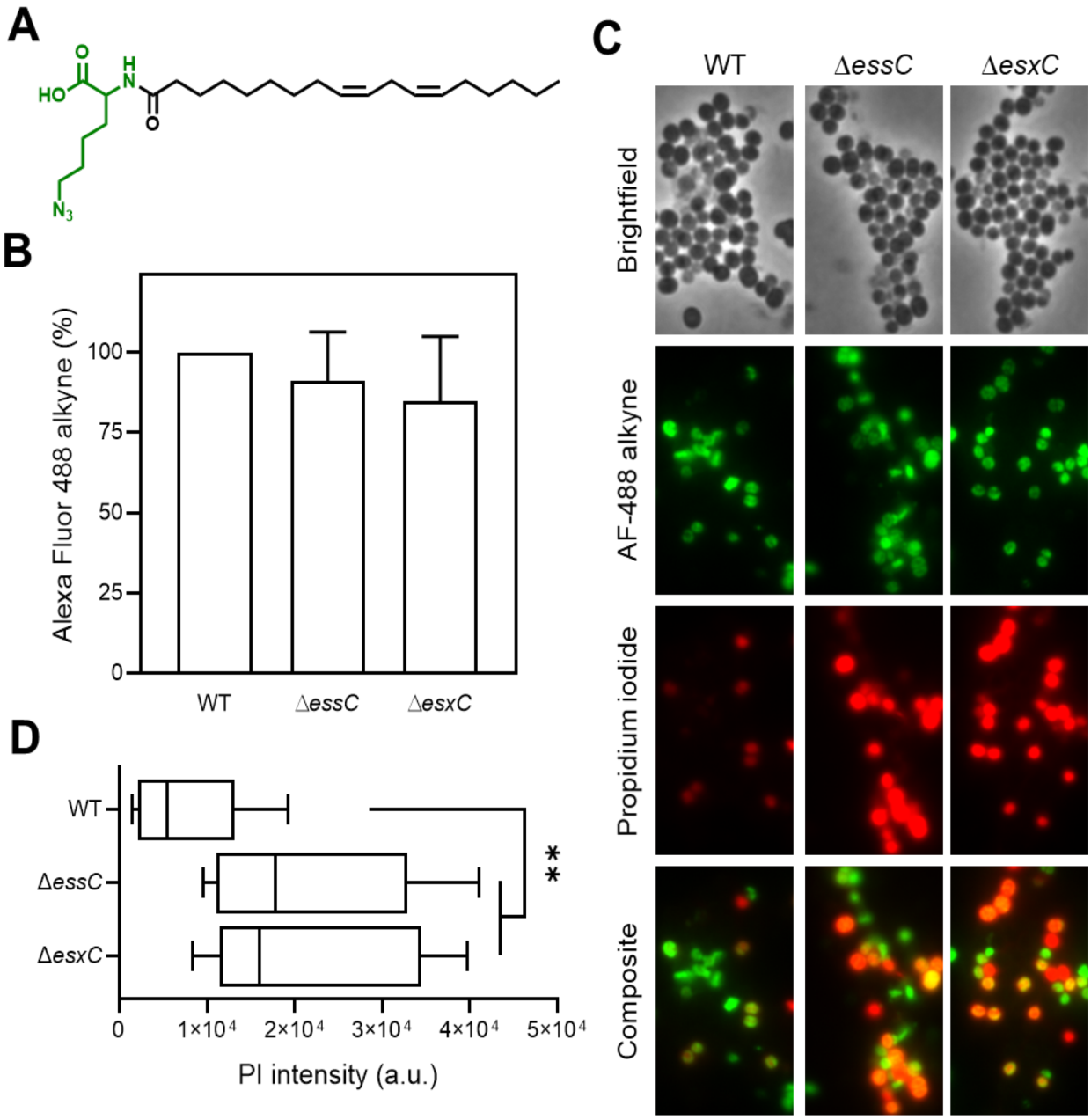
A
HO
O
H
N
O
N3
B
Alexa Fluor 488 alkyne (%)
100
75
50
25
0
WT
ΔessC
ΔesxC
C
WT
ΔessC
ΔesxC
Brightfield
AF-488 alkyne
Propidium iodide
Composite
D
WT
ΔessC
ΔesxC
**
0
1×10⁴
2×10⁴
3×10⁴
4×10⁴
5×10⁴
PI intensity (a.u.)

Fig 3

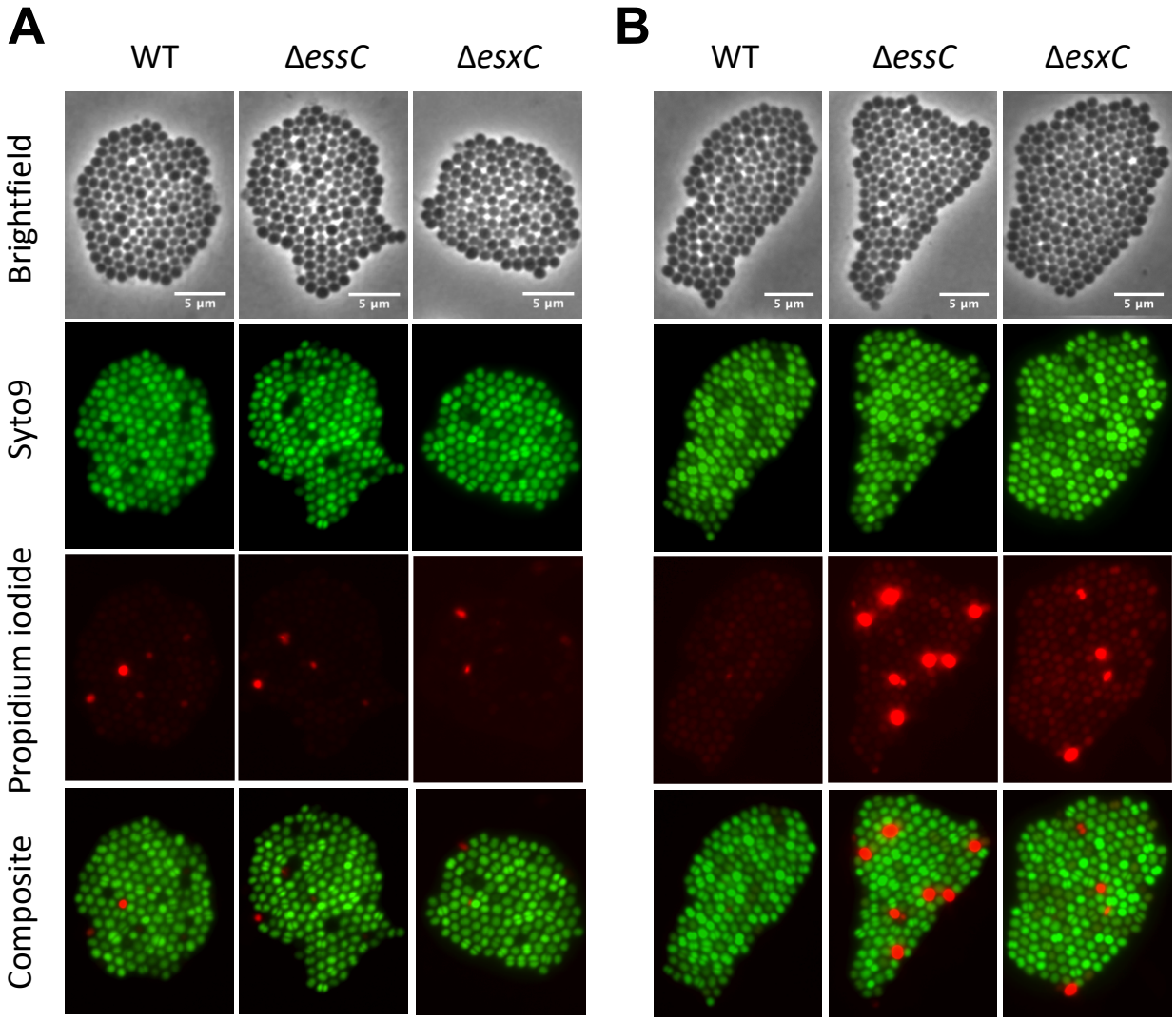
A
WT
ΔessC
ΔesxC
B
WT
ΔessC
ΔesxC
Brightfield
Syto9
Propidium iodide
Composite
5 µm

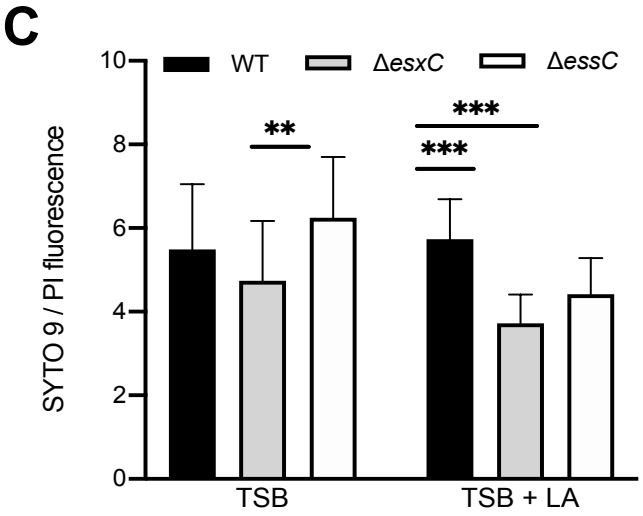
C
WT
ΔesxC
ΔessC
SYTO 9 / PI fluorescence
0
2
4
6
8
10
**
***
***
TSB
TSB + LA

Fig 4

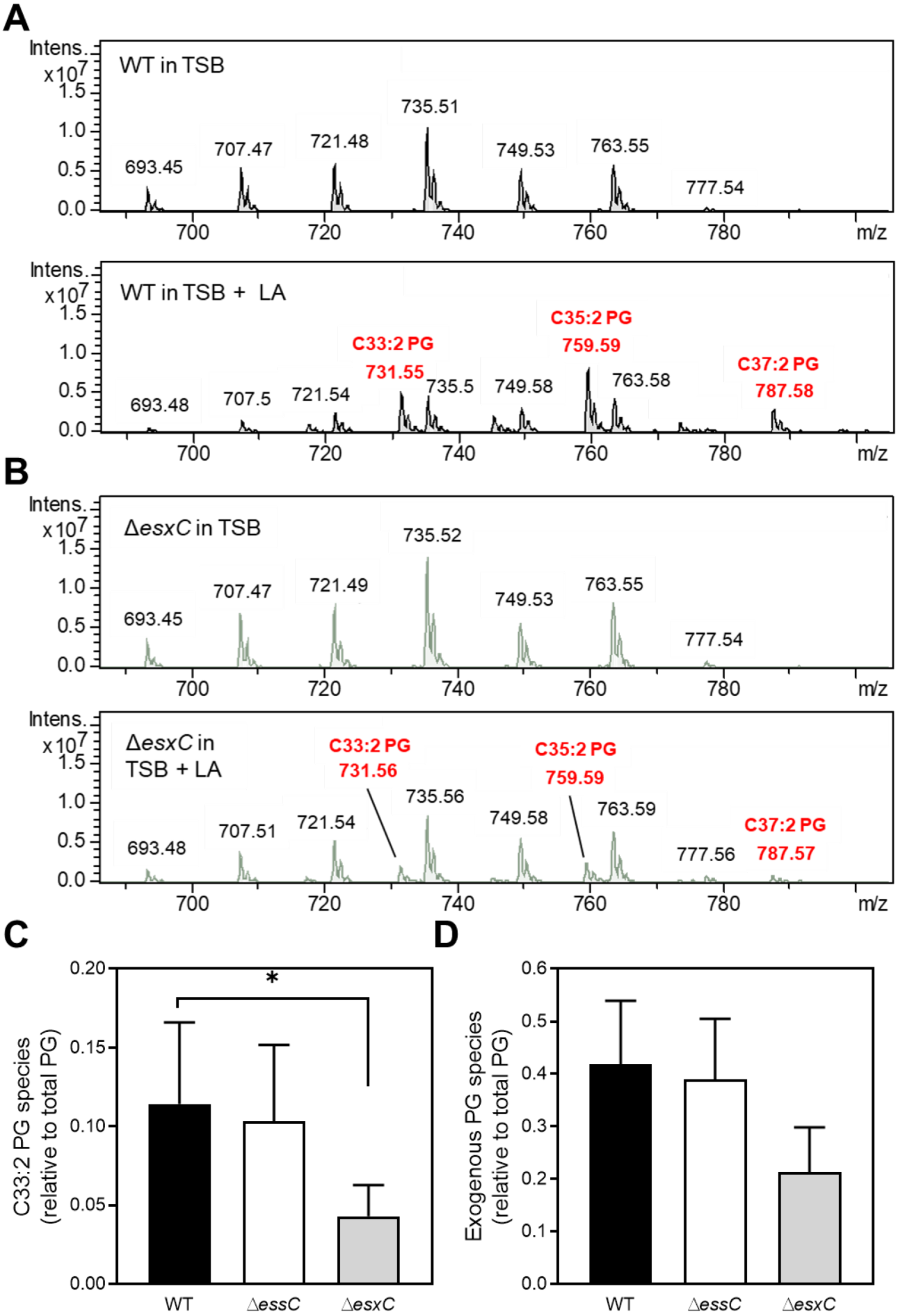
A
Intens.
x10^7
WT in TSB
693.45
707.47
721.48
735.51
749.53
763.55
777.54
m/z
WT in TSB + LA
C33:2 PG
731.55
C35:2 PG
759.59
C37:2 PG
787.58
693.48
707.5
721.54
735.5
749.58
763.58
B
ΔesxC in TSB
735.52
721.49
ΔesxC in
TSB + LA
C33:2 PG
731.56
C35:2 PG
759.59
C37:2 PG
787.57
693.48
707.51
721.54
735.56
749.58
763.59
777.56
C
C33:2 PG species
(relative to total PG)
*
WT
ΔessC
ΔesxC
D
Exogenous PG species
(relative to total PG)
WT
ΔessC
ΔesxC

Fig 5

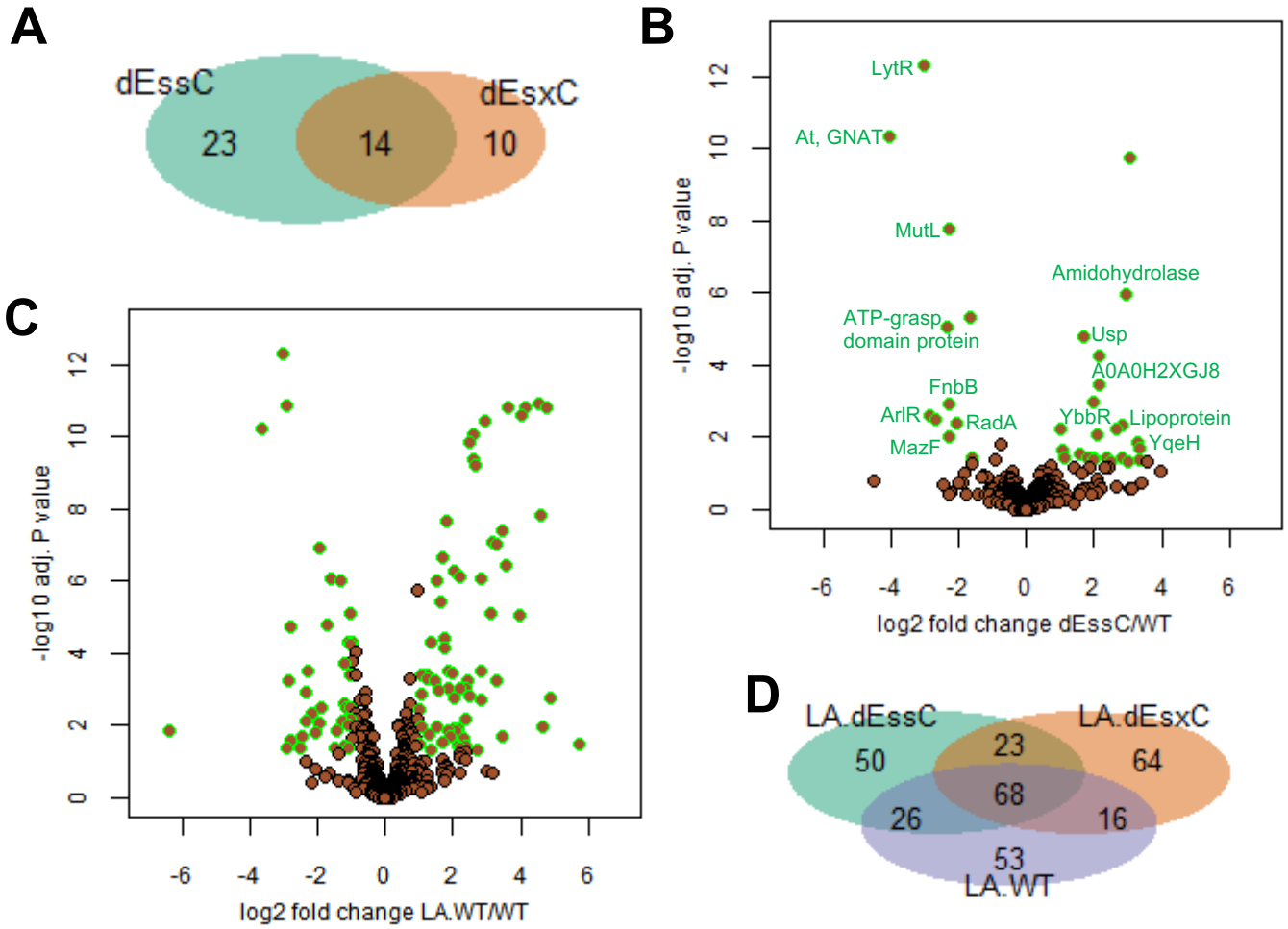
A
dEssC
dEsxC
23
14
10
B
LytR
At, GNAT
MutL
Amidohydrolase
ATP-grasp domain protein
Usp
A0A0H2XGJ8
FnbB
ArlR
RadA
MazF
YbbR
Lipoprotein
YqeH
-log10 adj. P value
log2 fold change dEssC/WT
C
-log10 adj. P value
log2 fold change LA.WT/WT
D
LA.dEssC
LA.dEsxC
LA.WT
50
23
64
68
26
16
53

Fig 6

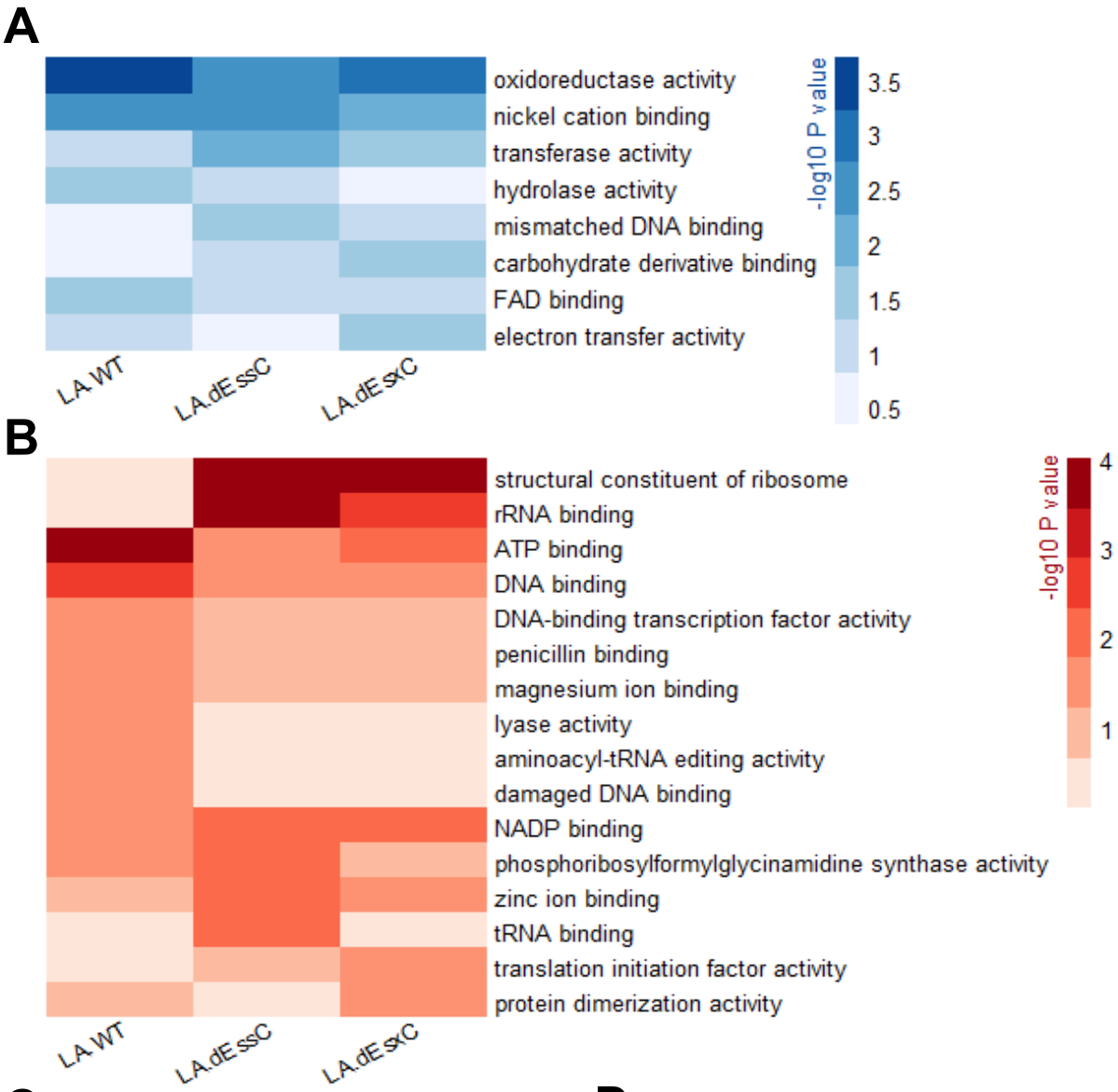
A
oxidoreductase activity
nickel cation binding
transferase activity
hydrolase activity
mismatched DNA binding
carbohydrate derivative binding
FAD binding
electron transfer activity
LA.WT
LA.dEssC
LA.dEsxC
-log10 P value
3.5
3
2.5
2
1.5
1
0.5
B
structural constituent of ribosome
rRNA binding
ATP binding
DNA binding
DNA-binding transcription factor activity
penicillin binding
magnesium ion binding
lyase activity
aminoacyl-tRNA editing activity
damaged DNA binding
NADP binding
phosphoribosylformylglycinamidine synthase activity
zinc ion binding
tRNA binding
translation initiation factor activity
protein dimerization activity
LA.WT
LA.dEssC
LA.dEsxC
-log10 P value
4
3
2
1

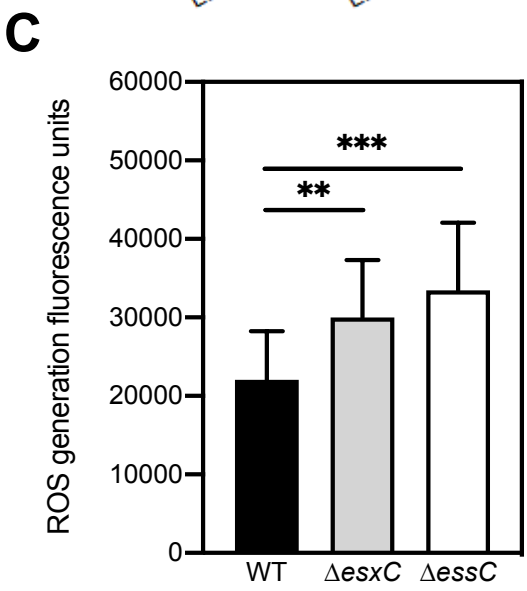
C
ROS generation fluorescence units
60000
50000
40000
30000
20000
10000
0
***
**
WT
ΔesxC
ΔessC

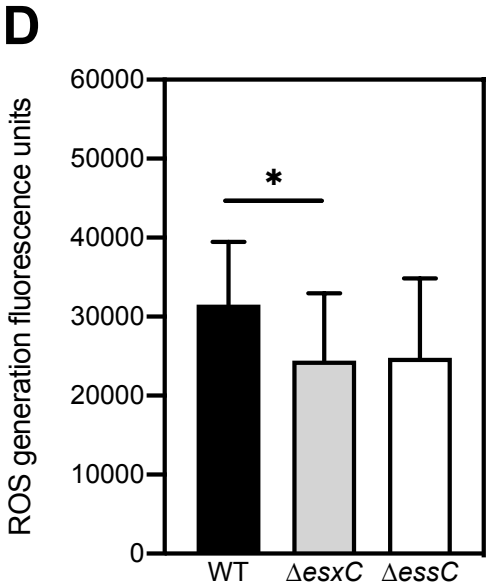
D
ROS generation fluorescence units
60000
50000
40000
30000
20000
10000
0
*
WT
ΔesxC
ΔessC

Fig 7